Published online 13 July 2022

Nucleic Acids Research, 2022, Vol. 50, No. 14 **8023–8040**
https://doi.org/10.1093/nar/gkac602

Enhanced polymerase activity permits efficient synthesis by cancer-associated DNA polymerase ε variants at low dNTP levels

Stephanie R. Barbari[1], Annette K. Beach[1], Joel G. Markgren[2], Vimal Parkash[2], Elizabeth A. Moore[1], Erik Johansson[2] and Polina V. Shcherbakova[1,*]

[1]Eppley Institute for Research in Cancer and Allied Diseases, Fred & Pamela Buffett Cancer Center, University of Nebraska Medical Center, Omaha, NE 68198, USA and [2]Department of Medical Biochemistry and Biophysics, Umeå University, SE-90187 Umeå, Sweden

Received April 19, 2022; Revised June 13, 2022; Editorial Decision June 20, 2022; Accepted June 29, 2022

ABSTRACT

Amino acid substitutions in the exonuclease domain of DNA polymerase ε (Polε) cause ultramutated tumors. Studies in model organisms suggested pathogenic mechanisms distinct from a simple loss of exonuclease. These mechanisms remain unclear for most recurrent Polε mutations. Particularly, the highly prevalent V411L variant remained a long-standing puzzle with no detectable mutator effect in yeast despite the unequivocal association with ultramutation in cancers. Using purified four-subunit yeast Polε, we assessed the consequences of substitutions mimicking human V411L, S459F, F367S, L424V and D275V. While the effects on exonuclease activity vary widely, all common cancer-associated variants have increased DNA polymerase activity. Notably, the analog of Polε-V411L is among the strongest polymerases, and structural analysis suggests defective polymerase-to-exonuclease site switching. We further show that the V411L analog produces a robust mutator phenotype in strains that lack mismatch repair, indicating a high rate of replication errors. Lastly, unlike wild-type and exonuclease-dead Polε, hyperactive variants efficiently synthesize DNA at low dNTP concentrations. We propose that this characteristic could promote cancer cell survival and preferential participation of mutator polymerases in replication during metabolic stress. Our results support the notion that polymerase fitness, rather than low fidelity alone, is an important determinant of variant pathogenicity.

INTRODUCTION

Replicative DNA polymerases ε (Polε) and δ (Polδ) synthesize the bulk of DNA on the leading and lagging strands, respectively, with high fidelity (1–4). This is achieved through correct nucleotide selection, exonucleolytic proofreading of errors and post-replicative DNA mismatch repair (MMR). Although the primary role of replicative polymerases is to synthesize new DNA, the ability to proofread is crucial to avoid disease-causing mutations. The polymerase must maintain these two enzymatic activities at an optimal ratio to ensure high replication efficiency and accuracy: excessive proofreading will slow replication while reduced proofreading and/or increased polymerase activity will cause error-prone synthesis (5). Proper levels of dNTPs during S-phase are also essential for replication fidelity and genome stability (6–9). Increased dNTP pools can hamper polymerase base selectivity, leading to a high rate of mutations (10–12). Likewise, reduced levels of DNA precursors can cause genome instability in part through a block in replication that triggers the recruitment of error-prone translesion DNA polymerases (7,13,14).

Heterozygous missense mutations affecting the exonuclease domain of Polε are associated with ultramutated cancers (15–18). These mutations occur at several hotspots, with P286 and V411 residues most frequently altered (18). While the mutations were initially presumed to simply abolish Polε exonuclease activity, *in vivo* and *in vitro* studies found that the consequences to polymerase function are variable and affect more than proofreading alone (19–25). For example, Polε variants modeled in yeast produced a range of mutator phenotypes with most exceeding that of the *pol2-4* mutant which lacks proofreading due to alanine substitutions at the catalytic residues D290 and E292 (19,20,24). Additionally, unlike mice heterozygous for the $Pole^{e}$ allele encoding exonuclease-deficient Polε (26), mice heterozygous for $Pole^{P286R}$ and $Pole^{S459F}$ mutations modeling recurrent cancer-associated variants had robust tumor

*To whom correspondence should be addressed. Tel: +1 402 559 7694; Fax: +1 402 559 4651; Email: pshcherb@unmc.edu

phenotypes (21,23,25). Furthermore, previous work with a purified catalytic fragment of human Polε demonstrated that many cancer-associated variants have exonuclease defects (27); however, the extent of exonuclease deficiency does not correlate with the variant incidence in tumors or with the mutator phenotype in yeast. Detailed biochemical analysis of the four-subunit yeast Polε-P301R modeling human Polε-P286R showed that, in addition to having a marked exonuclease defect, Polε-P301R was a strikingly hyperactive polymerase (22). This characteristic conferred an increased ability to extend mismatched primer termini and synthesize on difficult DNA substrates compared to both wild-type (WT) and exonuclease-deficient (Exo$^-$) Polε (22). Structural analysis suggested that the bulky arginine side chain protrudes into the DNA binding cleft of the exonuclease domain, interfering with the proper positioning of the 3′ end of DNA (28). These findings led to a model wherein the increased polymerase activity results from the inability of Polε-P286R to accommodate the primer terminus in the exonuclease active site, which tips the balance away from proofreading and toward synthesis (22,28). How other recurrent cancer-associated Polε mutations affect the enzyme function is not fully understood. Particularly, the second most prevalent V411L variant remained a long-standing puzzle. Despite the strong evidence of pathogenicity in humans, it inexplicably failed to produce a detectable mutator phenotype in yeast (20,24), only minimal effects on exonuclease activity were seen in biochemical studies (27), and the structural impact was elusive.

Here, we use the four-subunit yeast Polε holoenzyme as a model to assess the biochemical consequences of cancer-associated variants V411L (yV426L), S459F (yS474F), F367S (yF382S), L424V (yL439V) and D275V (yD290V). As observed previously with the truncated human catalytic subunit (27), all variant holoenzymes have exonuclease defects, albeit to varying degrees ranging from minor to a complete loss of proofreading function. All common cancer-associated variants have increased polymerase activity, most notably on challenging DNA substrates. Remarkably, the analog of the Polε-V411L was an especially strong polymerase despite having nearly full exonuclease function, revealing clues to the basis of its pathogenicity. Structural analysis suggested that the V411L analog (yV426L) affects a region important for primer transfer to the exonuclease site. We further show that the altered proofreading-polymerization balance in Polε-V411L analog strongly increases the rate of replication errors *in vivo*. These errors are efficiently corrected by MMR and, thus, were overlooked in previous studies that used MMR-proficient strains. Lastly, we show that, unlike WT Polε, hyperactive variants maintain strong activity at reduced dNTP concentrations, indicating efficient use of nucleotides. The resistance to dNTP depletion suggests that hyperactive Polε variants could benefit cancer cells during metabolic stress in two ways: first, by promoting survival, and second, by preferentially participating in DNA replication in heterozygous cells, thus enhancing the mutator and oncogenic phenotype. Together, our findings across multiple common Polε variants argue that, in addition to low fidelity, DNA polymerase fitness is likely a key determinant of variant pathogenicity.

MATERIALS AND METHODS

Saccharomyces cerevisiae strains and plasmids

The protease-deficient haploid strain FM113 (*MATa ura3-52 trp1-289 leu2-3,112 prb1-1122 prc1-407 pep4-3*) (29) was used to overproduce and purify WT yeast Polε. Exo$^-$ Polε and cancer-associated Polε variants were overproduced and purified from FM113 derivatives carrying the corresponding mutant allele (*pol2-4* (Exo$^-$), *pol2-P301R*, *pol2-S474F*, *pol2-F382S*, *pol2-L439V*, *pol2-D290V* or *pol2-V426L*) at the chromosomal *POL2* locus. These derivatives were constructed by replacing the chromosomal *POL2* with the mutant allele by transformation with the *URA3*-based integrative plasmids YIpJB1 (*pol2-4*) (30) or YIpDK1 containing the appropriate *POL2* mutation (19,20), followed by selection for the *URA3* marker on synthetic complete media lacking uracil and pop-out of the plasmid through counterselection on media containing 5-fluoroorotic acid. To overproduce four-subunit WT Polε for purification, FM113 was co-transformed with the galactose-inducible expression vectors pJL1, carrying *POL2*, and pJL6, carrying *DPB2, DPB3* and *DPB4* (31), followed by selection and maintenance on synthetic complete media lacking uracil and tryptophan. To overproduce mutant Polε variants, the mutations were introduced into the *POL2* gene in pJL1 by site-directed mutagenesis, and FM113 with the appropriate chromosomal *POL2* alleles were co-transformed with pJL1-*pol2-x* and pJL6.

To examine the interaction of *pol2-V426L* and *mlh1* deletion, the chromosomal *POL2* in E134 strain (*MAT*α *ade5-1 lys2-InsE$_{A14}$ trp1-289 his7-2 leu2-3,112 ura3-52*) was replaced with the *pol2-V426L* allele via transformation with YIpDK1-pol2-V426L (20) linearized with AgeI, followed by selection for clones that have lost the integrated plasmid on medium containing 5-fluoroorotic acid. *MLH1* in strain 1B-D770 (*MAT*a *ade5-1 lys2-Tn5-13 trp1-289 his7-2 leu2-3,112 ura3-4*) was disrupted with the *LEU2* gene using plasmid p*mlh1*Δ-*LEU2* as described in (32). The single *pol2-V426L* and *mlh1*Δ mutants were crossed to generate diploids. The diploids were then sporulated and *pol2-V426L mlh1*Δ double mutant haploids were generated by tetrad dissection.

Purification of four-subunit Polε variants

Untagged Polε variants were purified from yeast overproducing all four subunits by conventional chromatography as described previously (22,31) with some modifications. Yeast was grown in three flasks containing 400 ml each of SCGLA (6.7 g/l yeast nitrogen base without amino acids, 1 g/l glucose, 30 g/l glycerol, 20 g/l lactic acid, amino acids as for synthetic complete, adjusted to pH 5.5 with sodium hydroxide) media lacking uracil and tryprophan (SCGLA-ura-trp) overnight with shaking at 30°C. The overnight culture was distributed evenly into 20 flasks containing 400 ml of SCGLA-ura-trp and grown for 24 h with shaking at 30°C. 400 ml of YPGLA (10 g/l yeast extract, 20 g/l peptone, 1 g/l glucose, 30 g/l glycerol, 20 g/l lactic acid, 20 mg/l adenine, adjusted to pH 5.5 with sodium hydroxide) was then added to each flask, the cultures were grown for

4 h, and solid galactose was added to a final concentration of 2%. After 6 h, wet yeast cells (∼100 g) were harvested by centrifugation, resuspended in 36 ml of water, and frozen dropwise in liquid nitrogen. Frozen yeast pellets were disrupted using the SPEX SamplePrep 6870 Freezer/Mill (SPEX SamplePrep, USA). All remaining steps were carried out at 4°C. The disrupted yeast was thawed, the volume measured, and a 5× stock of buffer A (150 mM Tris-acetate, pH 7.8, 50 mM sodium acetate (NaAc), 2 mM ethylenediaminetetraacetic acid (EDTA), 1 mM ethyleneglycoltetraacetic acid (EGTA), 10 mM sodium bisulfite, 1 mM dithiothreitol (DTT), 5 μM pepstatin A, 5 μM leupeptin, 0.3 mM phenylmethylsulfonyl fluoride, 5 mM benzamidine) was added to a final concentration of 1× followed by 0.023 g of ammonium sulfate per ml of extract gradually while stirring and 0.04 ml of 10% polyethylenimine dropwise per ml of extract. The mixture was stirred for 15 min and then centrifuged at 39 000 × g for 30 min. Ammonium sulfate was then added to the supernatant at 0.106 g/ml, followed by stirring for 45 min and centrifugation at 39 000 × g for 45 min. 0.055 g of ammonium sulfate was then added per ml of supernatant, followed by stirring for 45 min and centrifugation at 39 000 × g for 45 min. The supernatant was discarded and the precipitate containing Polε was resuspended in 50 ml of buffer B_{50} (25 mM HEPES–NaOH, pH 7.6, 10% glycerol, 1 mM EDTA, 0.5 mM EGTA, 0.005% Nonidet P-40, 1 mM DTT, 5 μM pepstatin, 5 μM leupeptin, 5 mM benzamidine, 5 mM sodium bisulfite and 50 mM NaAc; the subscript for buffer B indicates the concentration in mM of NaAc in the buffer), flash frozen in liquid nitrogen and stored at –80°C. The next day, the sample was thawed and dialyzed in snakeskin dialysis tubing (ThermoFischer Scientific) against 2 l of buffer B_0 for 2 h, followed by centrifugation at 39 000 × g for 30 min. The supernatant was diluted 2-fold with buffer B_0, filtered, and loaded onto a 20-ml SP column (GE, USA) equilibrated with buffer B_{200} using a peristaltic pump. The column was washed with buffer B_{200} and protein was eluted in 2-ml fractions with a 60-ml B_{200}–B_{750} gradient using an AKTA FPLC (GE, USA). Peak fractions were combined, filtered, and loaded by peristaltic pump onto a 5-ml HiTrapQ column (GE, USA) equilibrated with buffer B_{540}. The loaded column was connected to the AKTA FPLC, washed with B_{200}, and protein was eluted in 1-ml fractions with a 40-ml gradient of B_{200} to B_{1200}. Peak fractions were pooled, diluted 2-fold with B_0, and injected into a 1-ml Mono S column (GE, USA) prewashed with buffer B_{100}. Protein was eluted by a 30-ml gradient of B_{100} to B_{1200} and 0.5-ml fractions were collected. The top two peak fractions were pooled, concentrated using an Amicon Ultra-0.5-ml 3K centrifugal filter (Millipore, USA), and injected into a Superdex 200 10/300 GL gel filtration column (GE, USA) prewashed with buffer C (25 mM HEPES–NaOH pH 7.6, 10% glycerol, 1 mM EDTA, 0.005% Nonidet P-40, 400 mM NaAc, 5 mM DTT, 2 μM pepstatin A, 2 μM leupeptin, 5 mM sodium bisulfite). 0.25-ml fractions were collected. Peak fractions were aliquoted into low-protein-binding tubes (Eppendorf), flash frozen in liquid nitrogen, and stored at –80°C. Protein concentrations were measured by the Bradford assay using bovine serum albumin as standard and proteins were appropriately diluted at desired concentrations in buffer C immediately before use in reactions. Two independent preparations were obtained for each Polε variant.

Exonuclease and DNA polymerase assays

For use in exonuclease and polymerase reactions, oligonucleotide DNA substrates were made by annealing a 1:1 ratio of Cy5-labeled primer P50 (Cy5-5′-TGGAACTTTGTACGTCCAAAATTGAATGA CTTGGCCAACTACACTAAGTT-3′) or P51T (Cy5-5′-TGGAACTTTGTACGTCCAAAATTGAATGA CTTGGCCAACTACACTAAGTTT-3′) to 80-mer template T80 (5′-GGTTTTCTTATCGTATCACTTTT GCCCTGGAACTTAGTGTAGTTGGCCAAGTCA TTCAATTTTGGACGTACAAAGTTCCA-3′), T80a4T (5′- GGATTACGAAACGAAGCACATTAGCCCT GGAACTTAGTGTAGTTGGCCAAGTCATTCAAT TTTGGACGTACAAAGTTCCA-3′), or T80H (5′-GGTTTTCTT**GGGCAA**TCACTT**TTGCCC**TGGAACT TAGTGTAGTTGGCCAAGTCATTCAATTTTGGA CGTACAAAGTTCCA-3′) in 150 mM NaAc pH 7.8 by heating for 2 min at 92°C and slowly cooling to room temperature for 2–3 h. The BsaJI restriction site in T80 and T80H (see section below) is underlined and the 6-nt inverted repeat in T80H is bolded in the above sequences. Exonuclease activity was also assessed using the P50 single-stranded primer alone. 10-μl exonuclease reactions contained 0.05 mg/ml bovine serum albumin, 40 mM Tris–HCl pH 7.8, 125 nM NaAc pH 7.8, 1 mM DTT, 8 mM magnesium acetate ($MgAc_2$), and oligonucleotide substrate and Polε at the indicated concentrations. For DNA polymerase assays, reactions also included dNTPs at S-phase concentrations (30 μM dCTP, 80 μM dTTP, 38 μM dATP, 26 μM dGTP) (33) unless indicated otherwise. Reactions were incubated at 30°C for the times indicated. To distinguish between proofreading and mismatch extension in reactions where the primer had a non-complementary 3′ end, the reaction products were digested with 10 units of BsaJI at 60°C for 1 h. Reactions were quenched on ice by the addition of an equal volume of 2× loading buffer containing 95% deionized formamide, 25 mM EDTA, and 0.025% Orange G. After boiling for 10 min and cooling on ice, 6 μl of the mixture was subjected to electrophoresis in a 10% denaturing polyacrylamide gel containing 8 M urea in 1× TBE. The gel was scanned on a Typhoon fluorescence imager (GE Healthcare) and products were quantified using ImageQuant.

Mutation rate and spectra

The rate of spontaneous mutation to canavanine resistance (Can^r) and reversion of *his7-2* allele was measured by fluctuation analysis as previously described (20). For mutational spectra analysis, individual colonies of *pol2-V426L mlh1*Δ isolates were patched on rich yeast extract peptone dextrose medium supplemented with 60 mg/l adenine and 60 mg/l uracil, grown for two days at 30°, and replica-plated onto synthetic complete medium containing L-canavanine (60 mg/l) and lacking arginine to select for Can^r mutants. One Can^r colony was picked from each patch, and the *CAN1* gene was amplified by PCR and Sanger-sequenced.

Purification, crystallization, and data collection of V426L and L439V mutants of $Pol2_{CORE}$

The V426L and L439V mutations were introduced by site-directed mutagenesis into the pET28a vector containing the catalytic part of the Pol2 subunit of Polε ($Pol2_{CORE}$, residues 1–1187) (a kind gift from Aneel K. Aggarwal (34). The mutant proteins were purified as previously described in (28). The ternary complex (protein-DNA-dATP) of the mutants was formed with 11ddC/16 primer–template DNA in the presence of Ca^{2+} to inhibit DNA degradation by the exonuclease domain. The crystals were obtained using hanging-drop vapor diffusion technique under conditions containing 50 mM MES, 150 mM NaAc and 8% PEG20K in the reservoir. For data collection at –80°C the crystals were frozen in liquid nitrogen after it was equilibrated with the well solution containing 15% glycerol. The complete datasets for $^{V426L}Pol2_{CORE}$ and $^{L439V}Pol2_{CORE}$ were collected using ID23-1 beamline at ESRF (Grenoble, France) and BioMAX beamline at MaxIV (Lund, Sweden), respectively. The $^{V426L}Pol2_{CORE}$ and $^{L439V}Pol2_{CORE}$ crystals diffracted to 2.6 and 2.46 Å with different space groups P2 and C2 (Supplementary Table S1), respectively.

Structure determination and refinement

Phaser (35) was used to solve the structure of $^{V426L}Pol2_{CORE}$ and $^{L439V}Pol2_{CORE}$ by molecular replacement technique using 4m8o (36) as the molecular replacement model. The $^{V426L}Pol2_{CORE}$ dataset processed in P2 space group gave a Mathews coefficient (V_M) of 2.65 $Å^2$/Da with 53.5% solvent content, which suggested two ternary complexes in the asymmetric unit. Coot (37) and the Phenix package (38) were used for model building and refinement of the structures, respectively. The final refined structures contain >95% of residues in the most favored regions of the Ramachandran plot (Supplementary Table S1), and the model was validated by using Coot (37) and Mol Probity (39). PyMol was used to superimpose the structures. The crystal structures of $^{V426L}Pol2_{CORE}$ (PDB ID: 7r3y) and $^{L439V}Pol2_{CORE}$ (PDB ID: 7r3x) were superimposed with $Pol2_{CORE}$ (PDB ID: 6fwk) (28) with a root mean square deviation (r.m.s.d.) of 0.4 Å for 985 C_α atoms. Structural superimposition over the exonuclease domain of 6fwk (28) gave rmsd of 0.23 Å and 0.31 Å (214 C_α atoms) for $^{L439V}Pol2_{CORE}$ and $^{V426L}Pol2_{CORE}$, respectively. The overall structures of the exonuclease domains are thus not affected by the V426L or L439V change.

RESULTS

Purification of Polε variants

We purified four-subunit yeast Polε carrying S474F (hS459F), F382S (hF367S), L439V (hL424V), D290V (hD275V) and V426L (hV411L) amino acid substitutions, as well as WT Polε, Exo⁻ Polε and the previously studied Polε-P301R (hP286R). The altered amino acid residues are located in the exonuclease domain and are conserved between human and yeast Polε (Figure 1A).

We aimed to create a comprehensive picture of how variants with a range of mutator effects (20) impact Polε function. P301R, S474F, F382S, L439V, and D290V substitutions increased the mutation rate 150×, 30×, 17×, 5.2× and 2.3× over WT, respectively, and the magnitude of increase generally correlated with variant incidence in tumors (Figure 1B). The mutator effects of P301R, S474F, F382S and L439V exceed that of proofreading deficiency. In contrast, strains with the D290V substitution in the ExoI motif have the same mutator phenotype as the exonuclease-dead *pol2-4* mutant, which is unsurprising since D290V eliminates the same catalytic residue that is mutated in *pol2-4.* We hypothesized that the D290V substitution would not have any additional biochemical consequences beyond disrupting exonuclease activity and could help highlight differences between variants that confer mutator effects beyond proofreading deficiency and variants that do not. Of note, unlike other variants in this group, the human analog of L439V (hL424V) is frequently seen as a germline mutation in patients with congenital cancer predisposition. It appears to account for most cases of *POLE*-mutant familial cancer (18,40,41). The moderate mutator effect of L439V substitution in yeast (Figure 1B) cannot explain the uniquely high incidence of hL424V in the hereditary cancer syndrome; therefore, it was interesting to determine whether this variant had unique biochemical properties. The last variant we selected, V426L, was of high interest because of the scarcity of evidence for the functional consequences of this substitution despite several indications that the highly recurrent human analog (hV411L) is likely pathogenic. All tumors carrying the V411L mutation: (a) have extremely high mutation burdens characteristic of *POLE*-mutated tumors (27,42–44), (b) carry the mutational signature associated with *POLE* mutations (27,43,45), (c) are associated with high neoantigen load, high levels of tumor-infiltrating lymphocytes, and excellent prognosis, which is characteristic of ultramutated tumors with other *POLE* mutations (46–50), and (d) are exceptional responders to immunotherapy, similar to other *POLE*-mutated tumors (51,52). One report of colorectal cancer in a pediatric patient harboring a germline *POLE-V411L* mutation further suggested that the mutation could be highly pathogenic (53). The lack of evidence for a mutator phenotype in model systems was, therefore, puzzling and warranted a more thorough functional analysis.

The eight Polε variants were purified as four-subunit holoenzymes with the correct stoichiometry, indicating that interaction with accessory subunits was not affected by the mutations (Supplementary Figure S1). All Polε preparations contained similar fractions of active enzyme (see Supplementary Methods and Supplementary Figure S2).

Cancer-associated Polε variants have a range of exonuclease defects

We first assessed 3′→5′ exonuclease activity of Polε variants on single-stranded (P50, Figure 2A) and double-stranded primer-template (P50/T80, Figure 2B) oligonucleotide substrates. As expected from previous work (22,30,54), Exo⁻ Polε lacked exonuclease activity while Polε-P301R showed a severe, although not complete, proofreading defect compared to WT Polε. Predictably, the ExoI motif variant Polε-D290V was exonuclease-dead due to the disruption of a catalytic residue. Polε-S474F was also completely de-

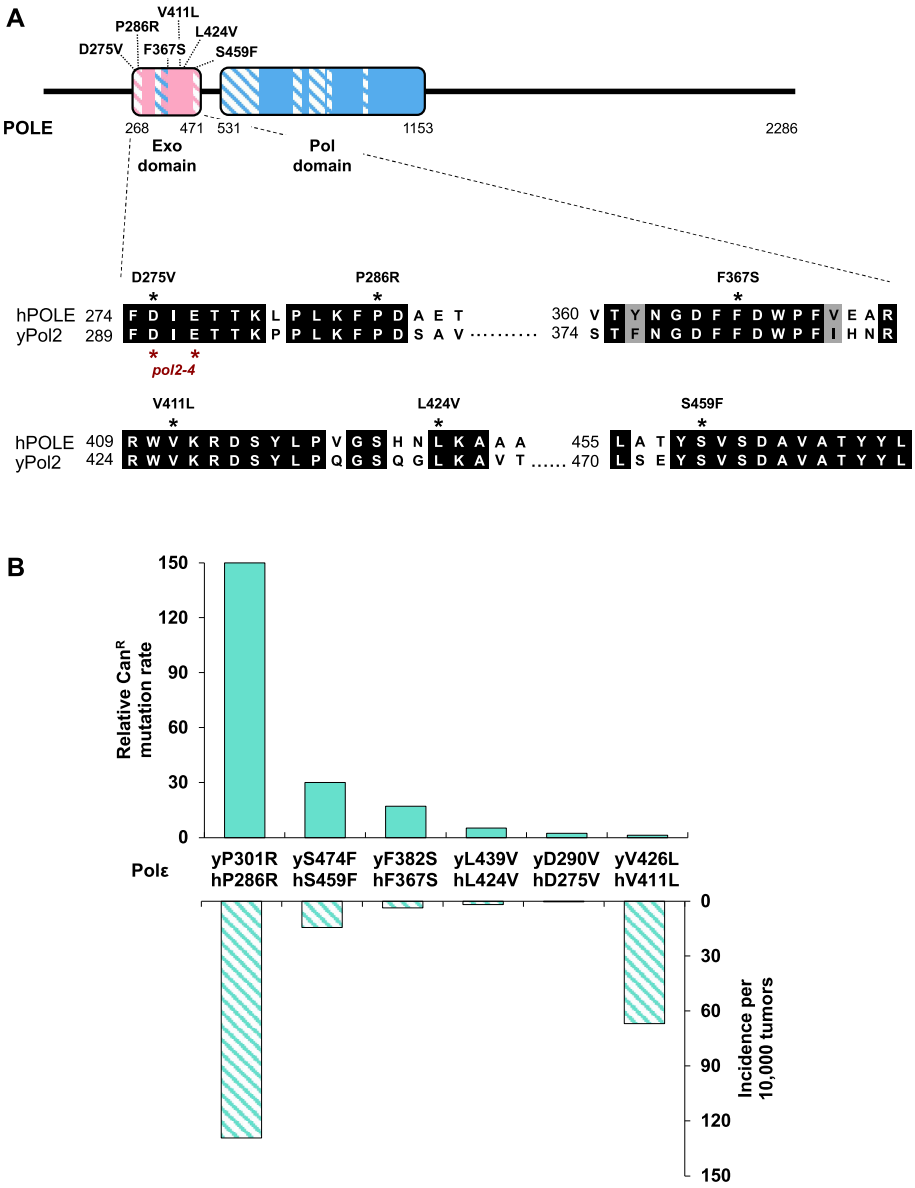

Figure 1. Characteristics of cancer-associated Polε variants used for biochemical studies. (**A**) Schematic of POLE showing the location of variants studied in this work with the alignment of amino acid sequences of human POLE and yeast Pol2 surrounding the mutation sites shown below. All variants occur at highly conserved residues in the exonuclease domain. (**B**) The mutator effect of each variant modeled in *S. cerevisiae* is shown above the x-axis and incidence per 10 000 tumors is shown below. Mutation rate data are from (19) and (20). *POLE* variant frequency was calculated from published studies (>20 000 tumors; Supplementary Table S2).

void of exonuclease activity. The remaining variants, Polε-F382S, Polε-L439V and Polε-V426L, retained various degrees of exonuclease function, with higher activity observed on single-stranded (Figure 2A) compared to double-stranded (Figure 2B) DNA. For the variants that had residual exonuclease activity, the extent of exonuclease deficiency correlated with the mutator effects produced in yeast (Figure 1B). Polε-V426L lacking a detectable mutator effect retained the most exonuclease function, degrading nearly as much DNA substrate as WT Polε (Figure 2). Thus, the consequences of cancer-associated mutations for Polε exonuclease activity are highly variable, in agreement with results obtained with truncated human Polε variants (27). Furthermore, we see that Polε variant incidence in cancer and perceived pathogenicity does not directly correspond to the severity of the exonuclease defect. This is perhaps best exemplified by the completely exonuclease-dead Polε-D290V mimicking the rare human Polε-D275V variant and the nearly fully exonuclease-proficient Polε-V426L mimicking the highly recurrent Polε-V411L (Figure 1B).

Cancer-associated Polε variants have increased DNA polymerase activity

Previous work showed that the yeast Polε-P301R mimicking the recurrent human Polε-P286R had substantially increased DNA polymerase activity compared to WT Polε and Exo$^-$ Polε (22). We sought to determine whether this

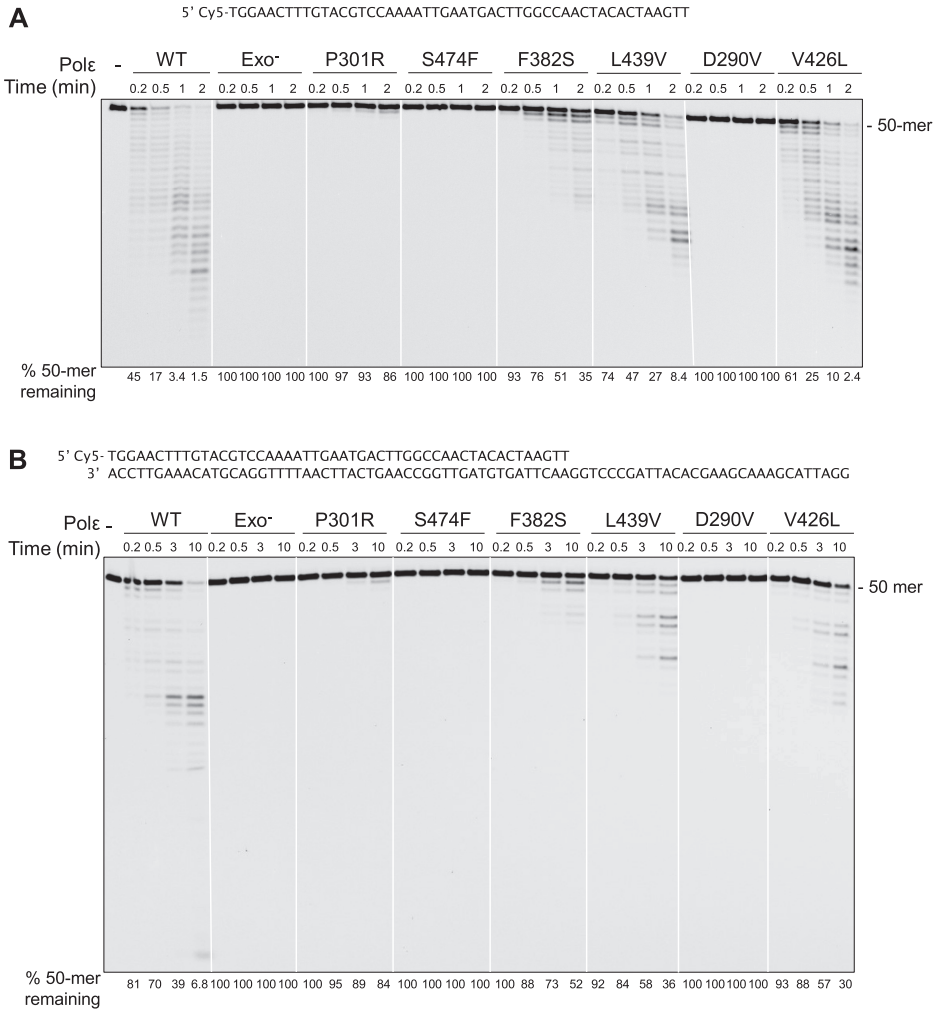

Figure 2. Exonuclease defects of cancer-associated Polε variants. Exonuclease activity was assessed using 25 nM P50 single-stranded (**A**) and P50/T80 partially double-stranded (**B**) oligonucleotide substrates and 3.125 nM Polε. Oligonucleotide sequences are shown above each gel. The fraction of 50-mer remaining is quantified below each lane. The gels shown are representative of three independent experiments. Cancer-associated Polε variants are in order of decreasing mutator effect starting with Polε-P301R as observed in (20).

property is shared by the multiple other Polε variants present in human tumors. We examined DNA synthesis by the Polε variants described above using the P50/T80a4T oligonucleotide substrate. Exo$^-$ Polε showed slightly higher activity than WT Polε, suggesting that the absence of proofreading *per se* is somewhat beneficial for synthesis on this DNA substrate (Figure 3A, B), likely because Exo$^-$ Polε does not undergo gratuitous cycles of nucleotide incorporation and excision. Markedly, nearly all cancer-associated Polε variants showed considerably higher polymerase activity compared to Exo$^-$ Polε, as seen by the greatly increased accumulation of full-length products (Figure 3A, B). Notably, Polε-V426L was one of the strongest polymerases despite having nearly full exonuclease activity, providing long-sought-after evidence of a prominent functional consequence of this variant. The fact that Polε-V426L shares the property of increased polymerase activity with the known recurrent pathogenic variants suggests that the increased activity may be relevant to the pathogenicity of the human V411L mutation. The ExoI motif variant Polε-D290V was the exception to other cancer-associated variants, having comparable polymerase activity to Exo$^-$ Polε (Figure 3A, B). This was not unexpected as the same catalytic carboxylate is altered in Polε-D290V and Exo$^-$ Polε. The greatly increased synthesis by variants that retain exonuclease activity (Polε-P301R, Polε-F382S, Polε-L439V, Polε-V426L) compared to Exo$^-$ Polε implies that the increased polymerase activity is a property separate from decreased proofreading and is not simply due to reduced nucleotide turnover. This is further illustrated by the poor correlation between exonuclease and polymerase activities among the Polε variants (Figure 3C).

Mismatch extension by cancer-associated Polε variants

Mutation generation during replication requires the insertion of an incorrect nucleotide to be followed by extension of the mismatched primer terminus. Replicative polymerase errors rarely lead to mutations in part because mismatch extension is much slower than proofreading. We pre-

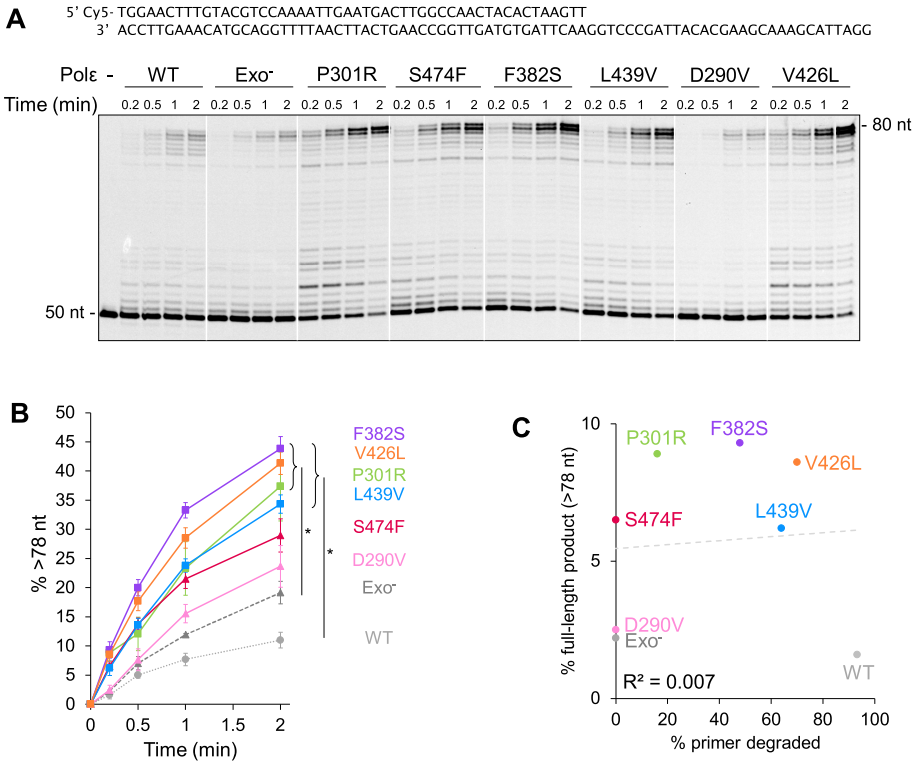

Figure 3. Increased DNA polymerase activity of cancer-associated Polε variants. (**A**) DNA polymerase activity was analyzed using 25 nM P50/T80a4T oligonucleotide substrate and 1 nM Polε. The oligonucleotide substrate sequence is shown above the gel. The gel is representative of three independent experiments. (**B**) The fraction of products greater than 78 nt was quantified (averages of three experiments). Error bars denote standard error. Asterisks indicate $P < 0.05$ as determined by one-way ANOVA with post-hoc Tukey test. (**C**) Lack of correlation between exonuclease and polymerase activities of Polε variants. Percent primer degraded at 10 min incubation (from Figure 2B) is plotted on x-axis, and percent full-length product at 0.2 min incubation (from panel A) is plotted on y-axis.

viously showed that the strong Polε-P301R mutator extends mismatched primer termini more efficiently than WT Polε and Exo$^-$ Polε (22). We sought to determine whether other cancer-associated mutator Polε variants had increased mismatch extension ability. The P51T/T80 primer-template substrate containing a 3′ terminal G–T mismatch was used in these experiments. Since most variants retain residual proofreading, full-length products could be produced on this substrate via extension of the mismatched primer or, alternatively, excision of the terminal T followed by extension of the resulting correctly matched primer. The P51T/T80 substrate contains a BsaJI restriction site at the primer-template junction that allows us to distinguish between these two outcomes (Figure 4; (22)). Products where the mismatched T is proofread are sensitive to BsaJI digestion, whereas extension of the mismatch destroys the restriction site and renders the products resistant to cleavage. To determine the propensity for each variant to extend *vs.* excise the mismatch, we first incubated Polε with the P51T/T80 substrate at a 1:8 ratio in the presence of normal S-phase dNTP concentrations for 30 min to allow for complete processing of all available substrate. BsaJI digestion of products revealed that, among variants that retain exonuclease activity, only Polε-P301R extended the mismatched primer more frequently than WT Polε (Figure 4, left). 71% of products generated by Polε-P301R resulted from mismatch extension compared to just 10% in WT Polε reactions, as we previously observed (22). All other Polε variants retaining partial exonuclease function, Polε-F382S, Polε-L439V, and Polε-V426L, proofread the mismatch nearly as frequently as WT Polε, with 89%, 89% and 86% of products, respectively, resulting from proofreading followed by extension. Exonuclease-deficient variants Exo$^-$ Polε, Polε-S474F and Polε-D290V extended the mismatch in 100% of cases, as expected (Figure 4, left). The faint band at the 52-nt position after BsaJI digestion likely results from primer slippage leading to incorporation of an additional T across from the upstream A's, as discussed previously (22). A time course of BsaJI-resistant product accumulation, which allowed direct comparison of mismatch extension by Exo$^+$ and Exo$^-$ variants showed that all cancer-associated Polε variants extend mismatched primers more efficiently than WT Polε, but only Polε-P301R was significantly more efficient than Exo$^-$ Polε (Supplementary Figure S3). Together, these results indicate that with most Polε variants retaining residual exonuclease activity, proofreading is favored over mismatch extension at dNTP concentrations present in unperturbed S-phase.

The comparable mismatch extension capacity of Exo$^-$ Polε and the recurrent cancer variants was somewhat unexpected since mutator effects of these variants *in vivo* exceed that of the exonuclease-deficient *pol2-4* strain. We and others have shown previously that replicative DNA polymerase errors can activate cell cycle checkpoint leading to the ex-

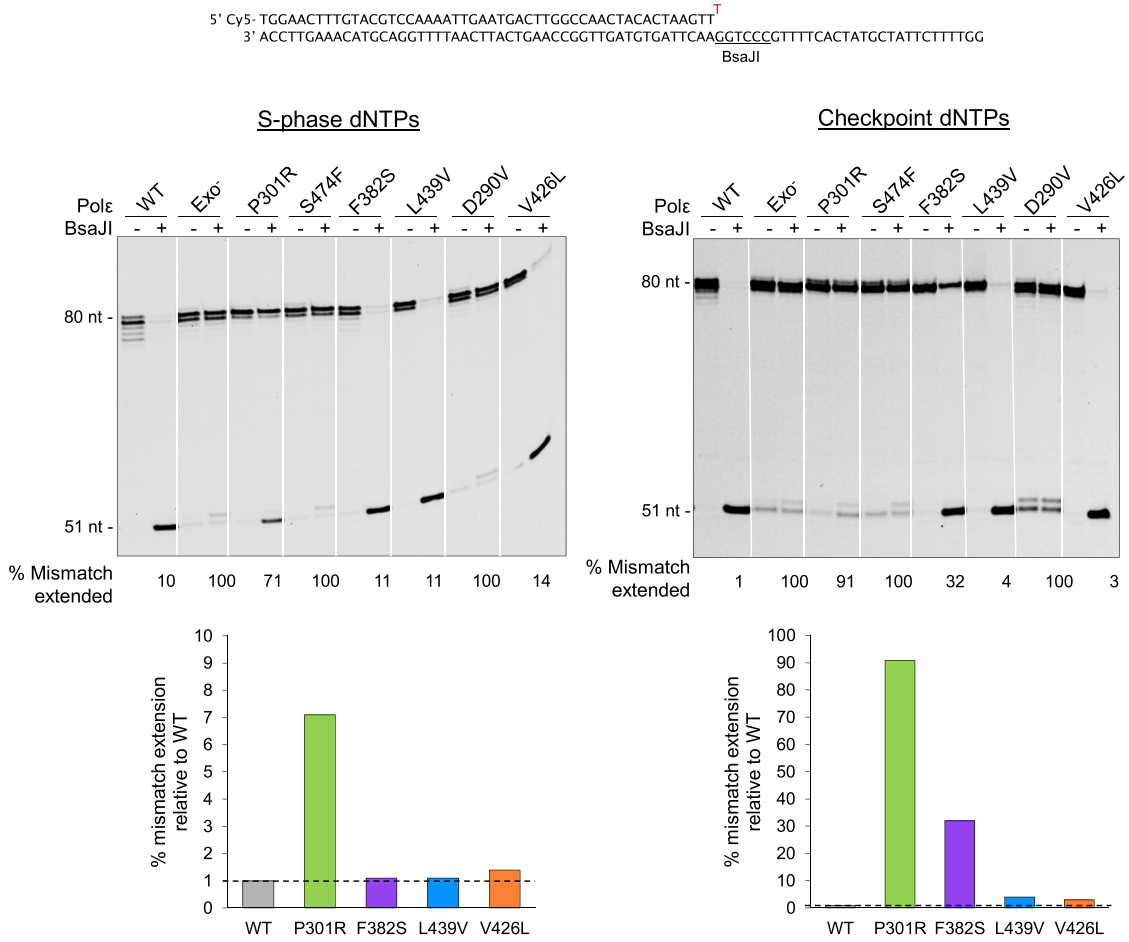

Figure 4. Mismatch processing by Polε variants. 3.125 nM Polε was incubated with 25 nM P51T/T80 containing a G-T mismatch at the 3′ primer terminus for 30 min at 30°C in the presence of dNTP concentrations corresponding to S-phase (*left*) and checkpoint-induced (*right*) levels. The checkpoint dNTPs were as estimated in (33) (114 μM dCTP, 266 μM dTTP, 171 μM dATP, 91 μM dGTP). Products were digested with BsaJI to determine the fraction of mismatch correction *vs.* extension. The presence of a 51-nt band after restriction digest indicates mismatch correction; products >62-nt remaining after BsaJI digest indicate mismatch extension. The fraction of products > 62-nt in BsaJI-digested samples is shown below the gel. Area corresponding to 52- to 62-nt-long products was excluded from quantification, because these products represent termination of synthesis before the BsaJI restriction site sequence and the adjacent nucleotides are copied. Representative images of three independent experiments are shown. The percentage of mismatch extension events for cancer variants relative to the percentage of mismatch extension events in WT Polε reactions is plotted below each gel.

pansion of intracellular dNTP pools (33,55). We, therefore, determined the relative efficiency of mismatch extension *vs.* proofreading by Polε variants at dNTP concentrations present in yeast cells with a constitutively activated checkpoint (33). Mismatch extension by the cancer variants was greatly improved under these conditions, particularly for Polε-P301R and Polε-F382S, where 91% and 32% of products, respectively, represented mismatch extension, Figure 4, *right*. These results support the view that robust mutator phenotypes of cancer-associated Polε variants are mediated by the increased ability to extend mismatch primer termini and suggest that checkpoint activation could augment mutator activity.

Hyperactive Polε variants efficiently bypass secondary structures

Certain repeat sequences, when present in single-stranded DNA during replication, repair, and transcription, can form non-B DNA structures such as hairpins, triplexes, and G quadruplexes (56). These secondary structures can impede replication and lead to genomic instability. DNA polymerases are expected to frequently encounter transient hairpin structures produced by short inverted repeats, which are abundant in the human genome (57). We previously showed that hairpin structures with stems as short as 4- to 6-nt can impede replicative polymerases *in vitro* (22,58) and that the hyperactive Polε-P301R is capable of bypassing such structures (22). To test the ability of other cancer variants to bypass secondary structures, we examined DNA polymerase activity on the P50/T80H substrate with a template containing 6-nt inverted repeats predicted to form a hairpin 3 nt downstream of the primer terminus (Figure 5A). WT Polε was inhibited by the hairpin, primarily using its exonuclease activity to degrade the primer and generating only a small amount of full-length product. Exo$^-$ Polε showed greater hairpin bypass activity compared to WT Polε, as seen previously (22) and consistent with earlier studies showing that exonuclease inactivation improves strand displacement activity of Polε (59). The ExoI mo-

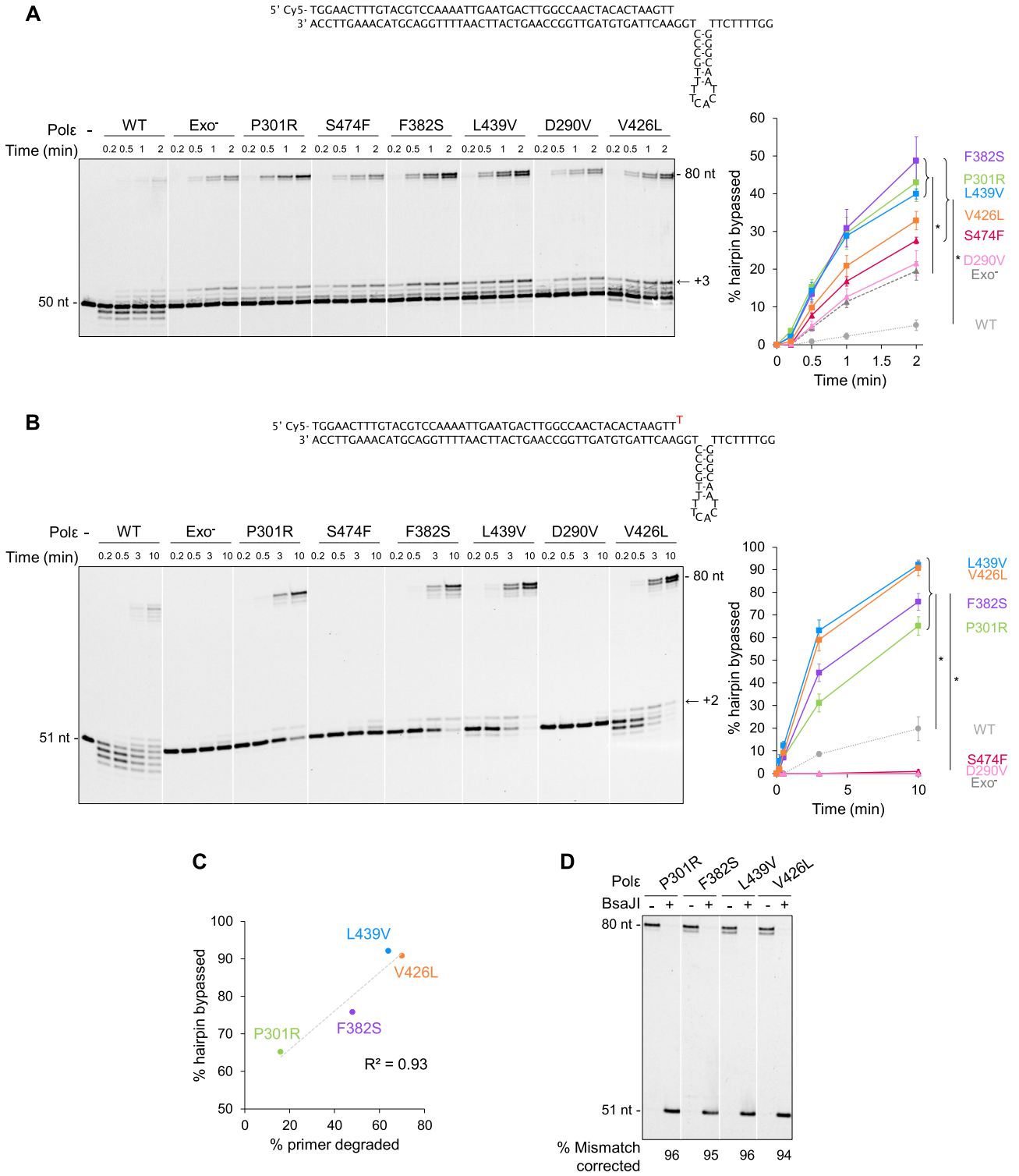

Figure 5. Bypass of hairpin DNA structures by Polε variants. (**A**) DNA polymerase activity was assayed using 2 nM Polε and 25 nM P50/T80H oligonucleotide substrate containing a 6-bp inverted repeat in the template, shown above the gel. A representative gel image from four independent experiments is shown. Hairpin bypass was quantified as the fraction of products greater than 71 nt and averages from four independent experiments are shown. Error bars denote standard error. Asterisks indicate $P < 0.05$ as determined by one-way ANOVA with post-hoc Tukey test. (**B**) DNA polymerase activity was assayed with 3.125 nM Polε and 25 nM P51T/T80H oligonucleotide substrate containing a G-T mismatch at the primer terminus and a 6-bp inverted repeat in the template, shown above the gel. A representative image from three independent experiments is shown. The fraction of products greater than 71 nt was quantified. Averages from three independent experiments are shown. Error bars denote standard error. Asterisks indicate $P < 0.05$ as determined by one-way ANOVA with post-hoc Tukey test. (**C**) The correlation between the percent of primer degraded in the exonuclease assay on P50/T80 substrate at 10 min incubation (x-axis, from Figure 1) and percent hairpin bypassed on P51T/T80H at 10 min incubation (y-axis, from panel B). (**D**) The relative efficiency of mismatch extension versus proofreading on P51/T80H was determined by incubating the DNA substrate with the polymerases for 30 min and digesting the reaction products with BsaJI as in Figure 4.

tif variant Polε-D290V produced similar amounts of full-length product to Exo⁻ Polε (Figure 5A). With all other cancer-associated Polε variants, the hairpin bypass was increased in comparison to Exo⁻ Polε, albeit to a variable degree. Polε-S474F and Polε-V426L showed moderately increased bypass, while Polε-F382S and Polε-L439V had significantly higher activity comparable to that of Polε-P301R (Figure 5A). Overall, the increased ability to copy alternatively structured DNA appears to be a common property of recurrent cancer-associated variants. The net efficiency of bypass is likely determined by the dynamic interplay of several factors. The first is the severity of the exonuclease defect, with exonuclease activity contributing to idling at the hairpin base and inhibiting bypass. The second is the increase in DNA polymerase activity, which promotes the bypass. For example, Polε-V426L has very strong polymerase activity but also powerful exonuclease activity; Polε-S474F is fully exonuclease-deficient but has somewhat lower polymerase activity than most cancer-associated variants; both Polε-V426L and Polε-S474F show only moderately increased hairpin bypass. In contrast, polymerase and exonuclease activities appear to be most optimally balanced for hairpin bypass in Polε-P301R, Polε-F382S, and Polε-L439V. In addition to the ratio of polymerase and exonuclease activities, Polε variant-specific interactions with the hairpin-containing DNA may also play a role in the efficiency of bypass.

We previously showed that the hyperactivity of Polε-P301R was best revealed on the challenging P51T/T80H substrate containing a G–T mismatch at the primer terminus and the putative hairpin in the template (22). Therefore, we investigated how other Polε variants process this difficult substrate. Synthesis by WT Polε was significantly blocked, and hydrolysis products predominantly formed, indicating enzyme idling at the hairpin base (Figure 5B). Synthesis by proofreading-deficient Exo⁻ Polε, Polε-S474F and Polε-D290V was completely hindered, as observed previously with Exo⁻ Polε (22). Conversely, like Polε-P301R, variants with residual exonuclease activity efficiently bypassed the hairpin and showed considerably higher activity compared to WT Polε (Figure 5B). Notably, the efficiency of hairpin bypass by cancer-associated Polε variants correlated with the amount of residual exonuclease (Figure 5C), with Polε-V426L being among the variants with the greatest activity (Figure 5B, C). Thus, residual proofreading in addition to increased polymerase activity provides an advantage on this DNA substrate. BsaJI digestion of the full-length reaction products showed that the mismatch was corrected approximately 95% of the time before synthesis proceeded (Figure 5D). These results underscore the powerful and versatile polymerizing properties of cancer-associated Polε variants that combine enhanced polymerase activity with the capacity to proofread.

Polε-V426L produces a strong mutator effect in MMR-deficient yeast

We and others found previously that *pol2-V426L* mimicking the highly recurrent and almost undoubtedly pathogenic *POLE-V411L* variant confers no detectable mutator phenotype in yeast (20,24). The lack of a mutator effect is even more perplexing in view of the biochemical data presented in the previous sections. While Polε-V426L retains nearly full exonuclease activity, the increase in DNA polymerase activity shifts the proofreading-polymerization balance severely toward polymerization. Polε-V426L performs significantly less hydrolysis than WT Polε even when synthesis is impeded by DNA secondary structures (Figure 5). DNA polymerases with a decreased proofreading-polymerization ratio are predicted to be mutators (5). We hypothesized that the mutator effect of *pol2-V426L* has been obscure because the earlier studies were conducted in MMR-proficient strains where the vast majority of Polε-V426L errors could be corrected. To determine whether the V426L substitution, in fact, increases the rate of replication errors *in vivo*, we studied the effects of *pol2-V426L* on the rate of spontaneous mutation in strains lacking *MLH1*. While *pol2-V426L* did not affect mutagenesis in the MMR-proficient control strain, the combination of *pol2-V426L* with the *mlh1* deletion resulted in a dramatic increase in the mutation rate over levels observed in the single *mlh1* mutant (Figure 6A, B; Supplementary Table S3). Thus, *pol2-V426L* mutation strongly reduces Polε fidelity *in vivo*. This observation reconciles the biochemical properties of Polε-V426L with its cellular effects and also resolves the discrepancy between the mutator studies in yeast and clinical data.

Other yeast *pol2* mutators also interact synergistically with MMR defects (20,60–65), consistent with the view that MMR corrects a majority of Polε errors. However, *pol2-V426L* represents an unusual case where MMR completely masks a fairly strong replication error phenotype. To determine what types of errors Polε-V426L generates, we characterized the spectrum of spontaneous *can1* mutations arising *in pol2-V426L mlh1*Δ strains (Figure 6C; Supplementary Figure S4). More than half of the mutations were single-base indels in poly(A)/poly(T) runs, which MMR is known to repair efficiently (60). An earlier study also noted an accumulation of indels in poly(A)/poly(T) runs in MMR-deficient *pol2-4* and *pol2-L439V* strains (24). A significant fraction of Polε-V426L-generated mutations, however, were base substitutions, primarily GC >AT transitions and GC >TA transversions at GG dinucleotides. This mutational specificity has been observed previously in replicative polymerase mutants and upon treatment of wild-type cells with mutagenic base analogs (33,66–69). To our knowledge, the efficiency of MMR at GG doublets has not been specifically assessed. In at least two experimental models where replication errors were amenable to MMR, base substitutions at GG sequences were still abundant in MMR-proficient cells (66,69), indicating that the corresponding mispairs are not completely removed. Thus, factors other than mutation type and DNA sequence context may contribute to the efficient correction of Polε-V426L errors.

V426L substitution affects a region important for primer transfer to the exonuclease site

It has been previously noted that the side chain of V426 is unlikely to contact the DNA bound in the exonuclease active site (20,43,70). Our finding of the robust exonuclease activity of Polε-V426L (Figure 2) is consistent with this view. Curiously, V426 is positioned in a conserved α-helix that is

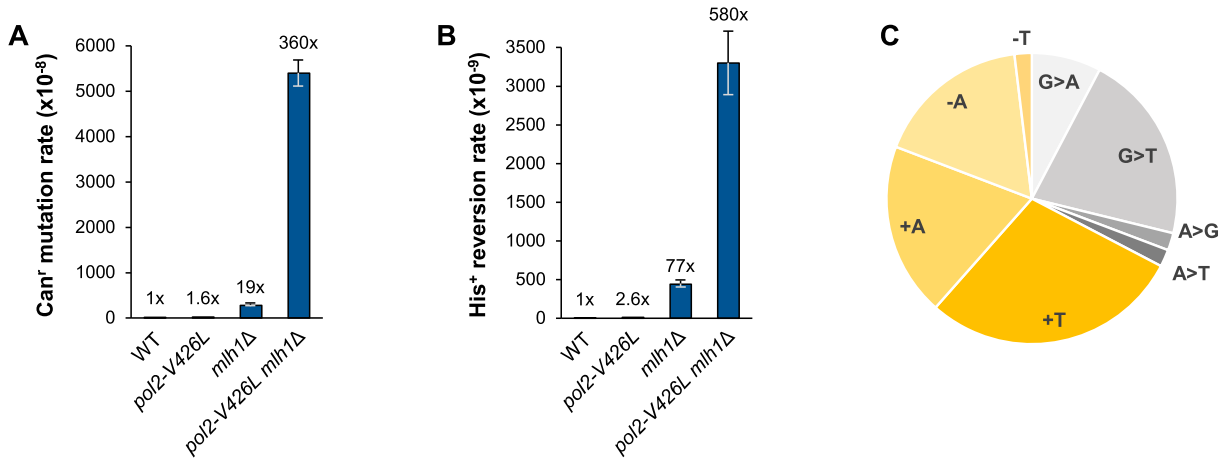

Figure 6. Synergistic interaction of *pol2-V426L* and MMR deficiency. (**A** and **B**) Rates of Can^r mutation and His$^+$ reversion in haploid yeast strains carrying chromosomal *pol2-V426L* and/or *mlh1*Δ alleles. Data are medians and 95% confidence intervals from Supplementary Table S3. Fold increases over the wild-type strain are shown above the bars. (**C**) The spectrum of spontaneous *can1* mutations in *pol2-V426L mlh1*Δ strain. Indels are shown in yellow and base substitutions in grey. The location of mutations in the *CAN1* sequence is shown in Supplementary Figure S4.

affected in an active-site-switching variant of T4 DNA polymerase isolated in a screen for polymerases with reduced dNTP turnover (71) (Supplementary Figure S5). This T4 Pol variant contains an insertion of an extra amino acid residue (Leu) between residues L271 and D272 and confers a mutator phenotype (71). We solved a crystal structure of the catalytic core of Polε-V426L (amino acids 1–1186) that contains both DNA polymerase and exonuclease domains. In the wild-type Polε, V426 is buried in a hydrophobic pocket, composed of W425, L432, F377, F423 and V442, which come from a helix-loop-helix motif (Figure 7A–C). The nine-residue-long loop provides a surface to interact with the DNA backbone, both in the polymerase and the editing mode (Figure 7B). These residues are centrally located between the polymerase and exonuclease active sites directly on the path that DNA must follow as it partitions between the two sites (Figure 7A, B). The V426L substitution does not introduce any significant structural changes in the surrounding residues, but it may reduce the flexibility to the helix-loop-helix motif, as the slightly more hydrophobic leucine packs tighter compared to valine (Figure 7C). A reduced flexibility of this region may impair the primer transfer to the exonuclease site.

Among other mutants we analyzed, Polε-L439V retained substantial exonuclease activity, and L439 is located in the second helix of the same helix-loop-helix motif that carries V426 (Figure 7B). Thus, we also investigated the structural impact of the L439V substitution. There are two possibilities by which L439V may influence Polε function. Firstly, the valine 439 does not reach as deep into a hydrophobic pocket as the leucine does (Figure 7D). This may affect the interaction between the helix and the core of the exonuclease domain, and that may in turn affect interaction between the loop region in the helix-loop-helix motif and single-stranded DNA during the transfer of DNA between the polymerase and exonuclease site. Secondly, compared to leucine, the valine is located closer to the DNA when bound in the exonuclease site and could possibly, through the hydrophobic properties, lower the affinity of the DNA for the exonuclease site (Figure 7E). This dual structural effect is consistent with the observation that the L439V substitution reduces the exonuclease activity of Polε more than V426L.

In summary, unlike other cancer-associated variants, V426L and L439V substitutions affect two helices of the same helix-loop-helix motif that appears to be involved in the efficient switch between the exonuclease and polymerase sites.

Hyperactive Polε variants tolerate low dNTP concentrations

The enhanced polymerase activity of cancer-associated Polε variants with reduced proofreading suggests that they efficiently use nucleotides rather than wasting them through repetitive dNTP insertion and excision. This was particularly evident on difficult DNA substrates (Figure 5 and (22)). We hypothesized that efficient nucleotide use by hyperactive Polε variants would facilitate DNA synthesis when dNTP supply is low. To test this hypothesis, we studied DNA polymerase activity on the P50/T80a4T substrate in the presence of decreasing concentrations of dNTPs while maintaining the S-phase dNTP ratio. All polymerases were mostly impervious to reduced nucleotides until levels reached half of normal concentrations (Figure 8). Upon further dNTP reduction, WT Polε became increasingly impaired, synthesizing half the amount of full-length products when dNTP concentrations dropped to 50% of S-phase levels and becoming nearly incapable of producing full-length products at 10% S-phase dNTPs (Figure 8). Exo$^-$ Polε and the ExoI motif variant Polε-D290V were more tolerant to reduced dNTP concentrations, remaining unaffected at 50% and 35% dNTPs and synthesizing approximately 15-fold and 10-fold more full-length product than WT Polε, respectively, at 20% dNTPs. Thus, the absence of proofreading *per se* is beneficial when dNTP levels are low. However, hyperactive cancer-associated variants were con-

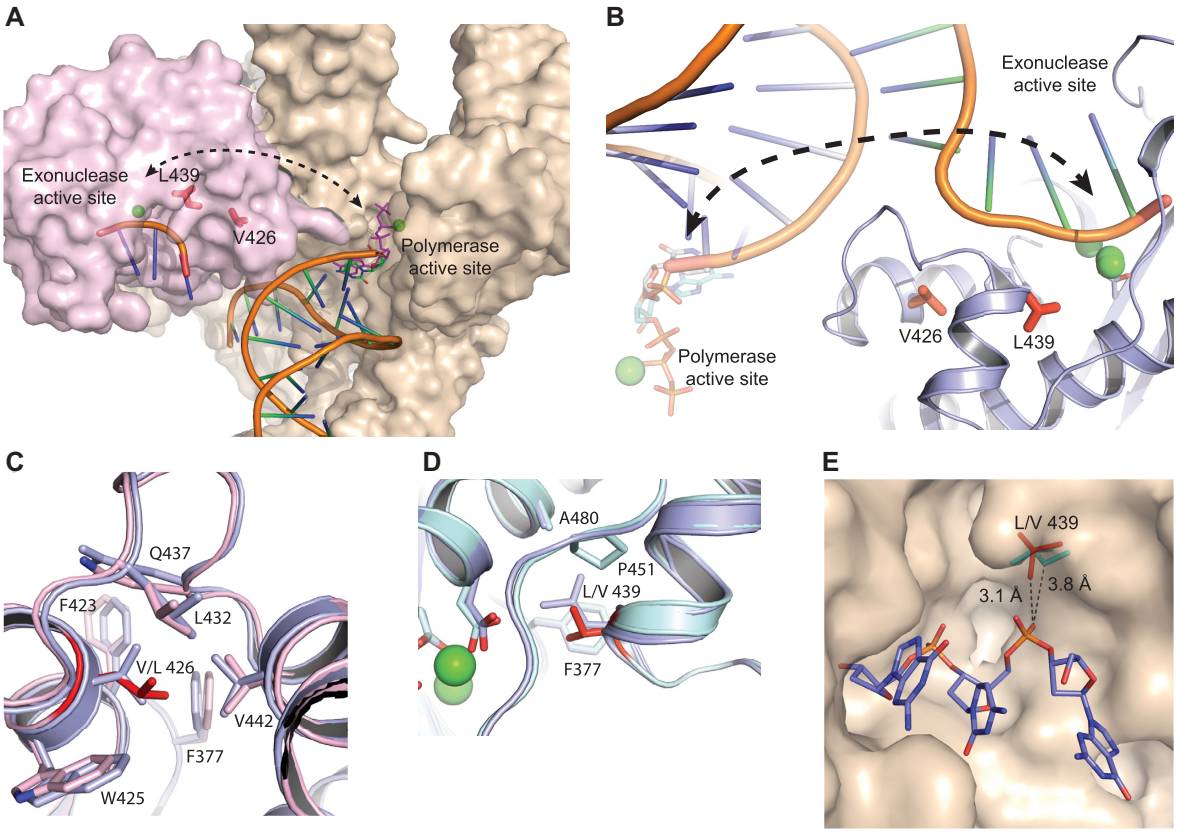

Figure 7. Insights from structures of Polε-V426L and Polε-L439V. (**A**) Surface representation of the finger and palm domain with the polymerase active site (light brown) and the exonuclease domain (pink) (PDB ID: 6fwk). DNA is shown in orange cartoon as it would bind to each active site. In the absence of a structure of Polε in the editing mode, the ssDNA was modelled into the exonuclease site of $Pol2_{CORE}$ by superimposing the exonuclease domain of a euryarchael B family DNA polymerase with single-stranded DNA bound in the exonuclease site (PDB ID: 4flw (86)). Amino acids L439 and V426 are shown in red sticks to illustrate that they are located in the trajectory for the switch of the primer terminus between the polymerase and exonuclease sites. (**B**) The V426 and L439 are located in a helix-loop-helix motif (blue) that is positioned where the primer terminus is transferred between the polymerase and exonuclease site. Metals bound to the active sites are shown in green. (**C**) The crystal structure of $^{V426L}Pol2_{CORE}$ (PDB ID: 7r3y) (pink) superimposed on the WT exonuclease domain of $Pol2_{CORE}$ (PDB ID: 6fwk) (blue). Amino acids V426 and L426 (red sticks) are buried in a hydrophobic pocket between the two helices of the helix-loop-helix motif that is located in the trajectory of the primer-end during the switch between the polymerase and exonuclease sites. (**D**) The crystal structure of $^{L439V}Pol2_{CORE}$ (PDB ID: 7r3x) (light blue) superimposed on the WT exonuclease domain of $Pol2_{CORE}$ (PDB ID: 6fwk) (blue) shows that L439 reaches further into a hydrophobic pocket when compared to V439. (**E**) Alignment of the WT exonuclease domain of $Pol2_{CORE}$ (PDB ID: 6fwk) and the exonuclease domain of $^{L439V}Pol2_{CORE}$ (PDB ID: 7r3x) shows that valine is located at a less favorable distance from the DNA, suggesting that DNA may have a lower affinity for the exonuclease site of Polε-L439V. The DNA (blue) is positioned based on an energy minimized MD simulation (28).

siderably more tolerant to reductions in dNTP concentrations compared to both WT Polε and Exo⁻ Polε. The most striking and significant differences were observed at 20% dNTPs, where Polε-P301R, Polε-F382S, Pol-S474F, Polε-L439V, and Polε-V426L synthesized approximately 46-fold, 44-fold, 30-fold, 29-fold and 26-fold more full-length products than WT Polε, respectively (Figure 8). Remarkably, Polε-P301R and Polε-F382S continued to maintain robust DNA synthesis when dNTP concentrations fell to 10% of normal levels and generated comparable amounts of full-length product to what WT Polε produced at physiological S-phase dNTPs (Figure 8). These data reinforce our conclusion that recurrent cancer-associated Polε variants are hyperactive at normal S-phase dNTP levels, and also reveal that the differences in activity between WT Polε and cancer-associated Polε variants are greatly amplified under conditions of replication stress.

DISCUSSION

Over a dozen mutations in the exonuclease domain of Polε are unequivocally associated with ultramutated tumors. It is evident from genetic and biochemical studies that the mutations alter more than just the proofreading function of the polymerase (19–22,24). What these additional consequences are remained unknown for most recurrent cancer-associated Polε variants. The biochemical analyses presented here demonstrate that the effects of mutations on Polε function are highly variable. Some Polε variants are completely devoid of exonuclease activity while many maintain residual proofreading function. Additionally, most Polε variants exhibit significantly increased DNA polymerase activity compared to WT Polε and Exo⁻ Polε, particularly on difficult DNA substrates containing replication-blocking hairpins. Strikingly, the cancer-associated Polε variants were profoundly resilient under

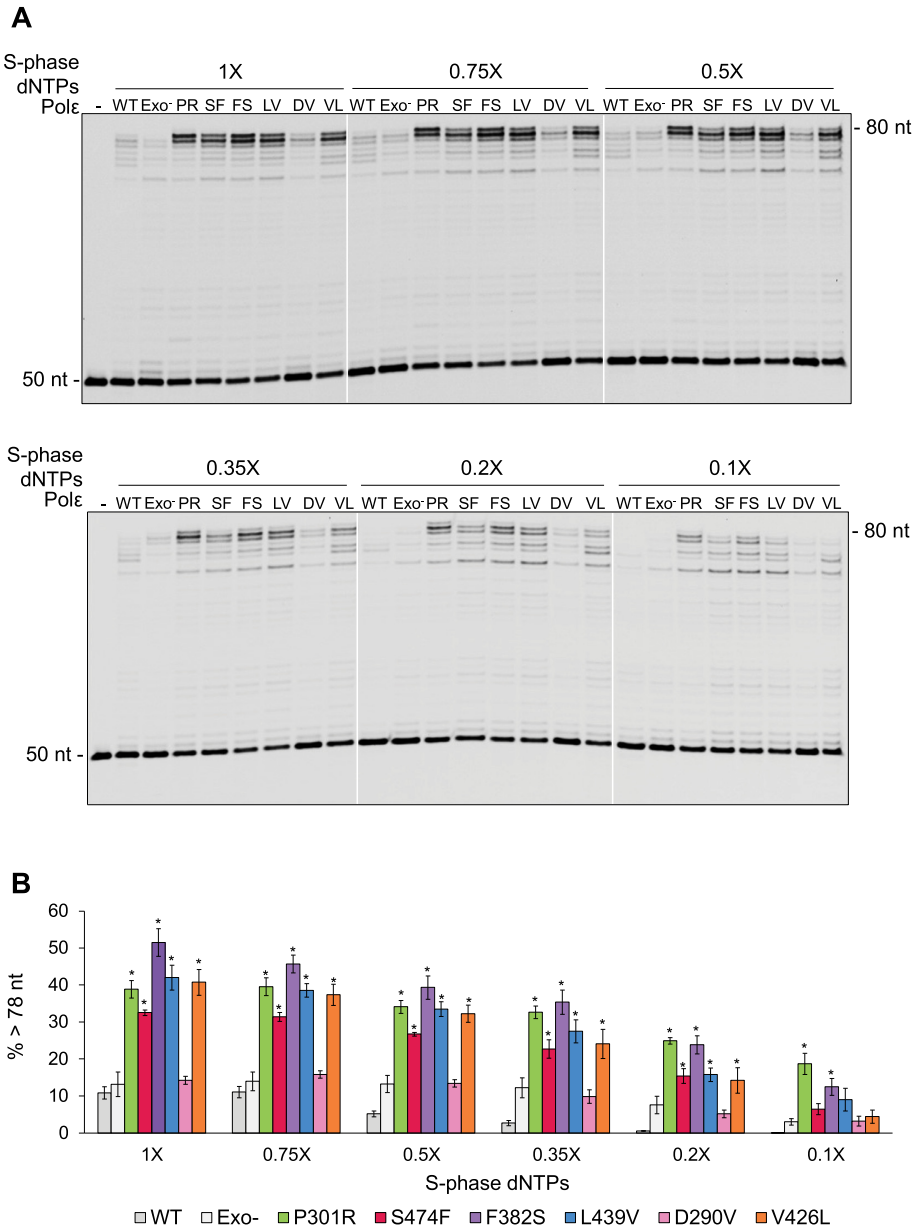

Figure 8. Efficient synthesis by cancer-associated Polε variants at reduced dNTP levels. (**A**) Reactions were performed with 25 nM P50/T80a4T oligonucleotide substrate and 1 nM Polε for 1 min. Fold changes in dNTP concentrations are indicated above the gel (the S-phase ratio of individual dNTPs was maintained in all reactions). A representative image from four independent experiments is shown. PR is Polε-P301R; SF is S474F; FS is F382S; LV is L439V; DV is D290V; and VL is V426L. (**B**) The fraction of products greater than 78-nt was quantified, and averages of four independent experiments were plotted. Error bars denote standard error. Asterisks indicate $P < 0.05$ compared to WT as determined by one-way ANOVA with post-hoc Tukey test.

conditions of reduced dNTP levels in stark contrast to WT Polε.

Detailed biochemical and structural analysis of Polε-P301R suggested a model wherein an increase in the polymerization/proofreading ratio results from protrusion of the bulky arginine side chain into the space typically occupied by the 3′-terminal nucleotide during proofreading. This impedes access of the DNA to the exonuclease active site and forces the polymerase to stay in the synthesis mode, thereby enabling efficient mismatch extension and, consequently, a strong mutator effect (22,28). In contrast, the catalytic residue variants Exo$^-$ Polε and Polε-D290V do not show a dramatic increase in polymerase activity or a high mutator effect. We proposed that, in the catalytically-dead enzymes, the primer terminus can still be partitioned from the polymerase active site to the exonuclease active site, which slows replication and prevents efficient mismatch extension (22). The increased polymerase activity of other cancer-associated Polε variants with residual proofreading (Polε-L439V, Polε-F382S, and Polε-V426L) suggests that, like Polε-P301R, they have a greater capacity to form polymerase complexes and a reduced ability to form exonuclease complexes. The precise mechanisms and extent of this shift, however, may differ among Polε variants depending

on the nature of the amino acid substitution and its location in the exonuclease domain. The structure of yeast Polε suggests that many amino acid residues altered in cancer, including L424 (yL439) and F367 (yF382), are positioned at the surface of the DNA binding cleft and could contact the DNA during proofreading (20). Changes to these residues are expected to affect the ability of the exonuclease domain to accommodate the primer terminus. The reduced capacity to form exonuclease complexes could be due to factors other than the mutated residue occupying too much space. For example, disruptions of DNA-protein interactions that aid in capturing or stabilizing the primer terminus in the exonuclease site could increase the rate of DNA partitioning back to the polymerase domain (5). In contrast, changes of residues that are not predicted to contact the DNA in the exonuclease site, such as V411L (yV426L) must alter the balance of synthesis and proofreading via indirect mechanisms. The location of V411 (yV426) in the α-helix known to be important for active site switching in T4 DNA polymerase ((71); (Supplementary Figure S5) and our structural data (Figure 7) suggest that the Leu substitution for V411 (yV426) in Polε could indirectly interfere with the transfer of DNA from the polymerase to the exonuclease active site. Our data on the greater propensity of Polε-V426L to polymerize despite robust hydrolysis capability further support the conclusion that the increased DNA polymerase activity is caused by a defect in polymerase-to-exonuclease active site switching.

The striking increase in polymerase activity exhibited by the Polε-V426L is an intriguing discovery, as previous studies have been unsuccessful in demonstrating any major functional consequences of this substitution. In yeast, Polε-V426L failed to produce a significant mutator phenotype in the presence of functional MMR (20,24). While the catalytic fragment of human Polε-V411L was previously shown to have a mild exonuclease defect (27), no evidence existed that the leucine substitution alters the accuracy of DNA synthesis. The lack of major functional effects was extremely puzzling as there is strong evidence to support pathogenicity of the V411L variant. It is one of the two prominent variants that are highly recurrent in tumors. V411L has also been reported as a germline mutation in a pediatric CRC patient (53). Tumors with the *POLE-V411L* allele possess characteristics similar to those of other *POLE*-mutated tumors, including remarkably high mutation burdens, similar mutational signatures, very high patient survival rates, high immunogenicity, and exceptional response to immunotherapies (15,16,43,44,51,52,72–75). We provide evidence that yeast Polε-V426L fully shares the property of increased DNA polymerase activity with other recurrent cancer-associated Polε variants. In fact, Polε-V426L was one of the most hyperactive polymerases. This was particularly apparent on the P51T/T80H substrate containing a terminal mismatch and putative hairpin in the template, where Polε-V426L had dramatically higher hairpin bypass activity in comparison to WT Polε. The properties of Polε-V426L constitute, perhaps, the strongest argument for the idea that increased polymerase activity and not the loss of proofreading *per se* is an important determinant of Polε variant pathogenicity. Of note, although the mutator effect of *pol2-V426L* in MMR-deficient background provides long-awaited evidence that this variant affects replication fidelity *in vivo*, tumors carrying the *POLE-V411L* allele are microsatellite stable and thus presumed to have functional MMR (18,42,43). It is possible that transient or partial loss of MMR not discerned by current tumor genome analysis occurs in cells carrying *POLE-V411L* and drives ultramutation. MMR capacity could also be different in yeast and humans, which should be considered when assessing the mutator effects of cancer-associated DNA polymerase variants in the yeast model.

Because the mutator effects of most Polε variants in yeast exceeded that of Exo$^-$ Polε (19,20), we expected consequences distinct from a simple loss of proofreading. Indeed, unlike Exo$^-$ Polε, most variants retained some exonuclease activity and had increased DNA polymerase activity. One exception was Polε-S474F mimicking the moderately recurrent human S459F variant. Polε-S474F showed a complete loss of proofreading and only a modest increase in DNA polymerase activity. Polε-S474F was, however, different from the ExoI motif variants Exo$^-$ Polε and Polε-D290V in that it had higher DNA polymerase activity on most DNA substrates. Although the differences seen at normal S-phase dNTPs did not meet the cutoff for statistical significance, they were greatly amplified at reduced dNTP levels. Consistently, *pol2-S474F* allele was a much stronger mutator in yeast, with the mutation rate exceeding that of *pol2-4* and *pol2-D290V* by 15-fold (20). These results suggest that while Polε-S474F is incapable of hydrolysis, it may also have reduced ability to form exonuclease complexes compared to Exo$^-$ Polε and Polε-D290V, thus tipping the balance toward increased synthesis. It is possible that the modest increase in DNA polymerase activity and, presumably, mismatch extension combined with a complete exonuclease defect is sufficient to increase the error rate *in vivo*. Another possible explanation for the strong mutator effect is that Polε-S474F is deficient in nucleotide selectivity in addition to a loss of proofreading function. Indeed, the N-terminal fragment of human Polε-S459F was less accurate than the analogous Polε fragment with the catalytic residue substitution in the ExoI motif and produced a slightly different spectrum of errors during DNA synthesis *in vitro* (27). We consider this possibility less likely due to the location of the S459F (yS474F) substitution in the exonuclease domain away from the polymerase regions important for nucleotide selectivity.

Our findings highlight the role of the delicate balance between synthesis and proofreading in replication and how alterations to this balance yield hyperactive mutator polymerases that are selected for in cancers. The relationship between polymerase-exonuclease balance and the mutation rate has been extensively studied, beginning with the bacteriophage T4 DNA polymerase (76). Antimutator T4 polymerases have a reduced ability to form polymerase complexes, thus providing more opportunities for proofreading (77,78). On the other hand, mutator T4 polymerases result from reduced proofreading, either through the inability to perform hydrolysis or a reduced capacity to form exonuclease complexes (79,80) *or* through increased stability of polymerase complexes, increasing the ability to extend mismatches even in the presence of full exonuclease activity (81). These properties of bacteriophage DNA polymerases

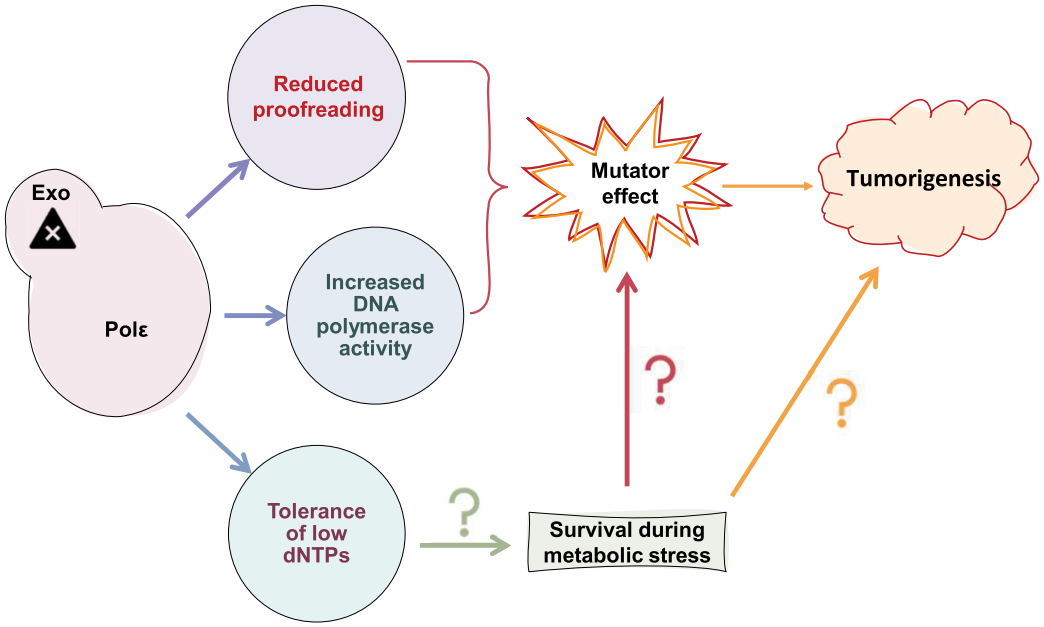

Figure 9. Summary of characteristics relating to the pathogenicity of Polε variants. Cancer-associated Polε variants have reduced proofreading and increased DNA polymerase activity, leading to decreased fidelity and a strong mutator effect. Hyperactive variants are also tolerant to reduced levels of dNTPs. Future studies will determine whether this characteristic can promote survival (green question mark) and mutagenesis (red question mark) during metabolic stress, with both pro-survival and pro-mutagenic roles contributing to tumorigenesis (orange question mark). Exo, exonuclease domain; Polε, polymerase domain.

are shared among DNA polymerases from many organisms, including eukaryotes (5). Our data shows that Polε variants selected for in cancers are hyperactive mutators resulting from a shift in the exonuclease/polymerase ratio via reduced exonuclease *and* increased polymerization. We found that the presence of exonuclease activity can be beneficial or detrimental for synthesis depending on the DNA substrate. For example, proofreading was necessary to generate full-length products on the DNA substrate with a terminal mismatch and a strong hairpin in the template (Figure 5B). On the other hand, too much proofreading can prevent efficient synthesis, as we observed for WT Polε on hairpin-containing DNA substrates (Figure 5). Altogether, we demonstrate that the dynamic interaction between polymerization and proofreading dictates how well Polε variants synthesize DNA in different sequence contexts. We find that enzymes with moderately reduced but not fully inactivated proofreading and increased polymerase activity are most optimally fit and versatile for efficient DNA replication, which may be important for cancer cell proliferation.

Perhaps the most striking observation from our studies was the extraordinary ability of hyperactive Polε variants to synthesize DNA at low dNTP concentrations, with Polε-P301R producing as much full-length product at ten-fold reduced dNTPs as WT Polε at normal dNTP concentrations (Figure 8). The increased synthesis at low dNTP levels must reflect, at least in part, increased affinity for the incoming dNTP and not just reduced consumption of nucleotides, because cancer-associated Polε variants with residual exonuclease activity decidedly outperformed exonuclease-dead Exo$^-$ Polε and Polε-D290V. These observations substantiate the notion that hyperactive Polε variants are fit enzymes that efficiently use nucleotides and may provide unique insights into the etiology of *POLE*-mutant cancers. The current model proposes that mutator *POLE* alleles arise early in cancer progression and lead to an elevated mutation rate, which increases the chance of accumulating mutations in oncogenes and tumor suppressor genes and, consequently, oncogenic transformation (44,82). Our findings uncover an additional potential role of *POLE* variants in promoting DNA replication under conditions of low dNTP pools. Nucleotide deficiency has been proposed to fuel replication stress in the early stages of cancer development (83). In another study, oncogene-induced senescence was shown to be established and maintained through the suppression of nucleotide metabolism, resulting in replication stress and senescence-induced cell cycle exit (84). dNTP levels ranging from less than 10% to about 25% of normal concentrations, depending on the nucleotide, were reported upon oncogene activation (84). We speculate that DNA synthesis by hyperactive Polε variants could be essential for cell survival when nucleotides are depleted. Additionally, cells heterozygous for *POLE* mutations could preferentially use the hyperactive error-prone Polε variants for DNA synthesis when dNTP pools are low, although high levels of mutagenesis may not occur until dNTP supply is restored to permit efficient mismatch extension. Indeed, we and others previously observed that downregulation of dNTP synthesis suppresses the mutator effect of error-prone Polδ and Polε variants (33,55,85, and our unpublished data). The oncogenic advantage provided by hyperactive Polε variants under metabolic stress could, therefore, stem from improved replication rather than mutagenesis.

In summary, we describe the biochemical properties of several Polε variants associated with ultramutated tumors (Figure 9). We demonstrate that the major consequences of

Polε mutations to enzyme function are reduced proofreading and greatly increased DNA polymerase activity, which is particularly evident on hairpin-containing DNA substrates. These factors likely promote the enhanced mutator effects previously observed in yeast cells carrying these variants. Additionally, we show that hyperactive variants are impressively tolerant to reduced levels of dNTPs, in stark contrast to WT Polε. Future studies are warranted to determine whether this characteristic can promote the survival of cells heterozygous for Polε mutations during metabolic stress. Additional studies could also determine whether mutator Polε variants preferentially participate in replication, thus increasing the mutator effect and driving tumorigenesis. These analyses could shed light on underappreciated roles of Polε variants in cancer that are distinct from reduced DNA polymerase fidelity.

DATA AVAILABILITY

Atomic coordinates for $^{V426L}Pol2_{CORE}$ and $^{L439V}Pol2_{CORE}$ crystal structures have been deposited to the Protein Data bank as PDB IDs: 7r3y and 7r3x. All other data necessary to support the conclusions are presented fully within the manuscript and supplementary material.

SUPPLEMENTARY DATA

Supplementary Data are available at NAR Online.

ACKNOWLEDGEMENTS

We thank Linda Reha-Krantz for inspiring email and personal discussions and critically reading the manuscript. We acknowledge MAX IV Laboratory for time on Beamline Biomax and the European Synchrotron Radiation Facility for provision of beam time on beamline ID 23-1.
Author contributions: S.R.B. purified four-subunit Polε variants and performed the biochemical analysis. A.K.B. studied the genetic interaction of *pol2-V426L* and *mlh1* mutations. A.K.B., E.A.M. and P.V.S. characterized the mutational specificity of *pol2-V426L mlh1* strains. P.V.S. supervised the biochemical and genetic studies. J.G.M and V.P. purified the catalytic core of Pol2-V426L and Pol2-L439V (amino acids 1–1186) and solved their structures. J.G.M, V.P. and E.J. analyzed the structures. E.J. supervised the crystallographic studies. S.R.B. and P.V.S. wrote the manuscript with input from all authors. All authors read and approved the manuscript.

FUNDING

National Institutes of Health [ES015869, CA239688 to P.V.S.]; Swedish Cancer Society and Swedish Research Council (to E.J.); research conducted at MAX IV, a Swedish national user facility, is supported by the Swedish Research Council [2018-07152]; Swedish Governmental Agency for Innovation Systems [2018-04969]; Formas [2019-02496]. Funding for open access charge: National Institutes of Health [CA239688].
Conflict of interest statement. None declared.

REFERENCES

1. Morrison,A., Araki,H., Clark,A.B., Hamatake,R.K. and Sugino,A. (1990) A third essential DNA polymerase in *.S. cerevisiae*. *Cell*, **62**, 1143–1151.
2. Kunkel,T.A. (2004) DNA replication fidelity. *J. Biol. Chem.*, **279**, 16895–16898.
3. Ganai,R.A. and Johansson,E. (2016) DNA replication—a matter of fidelity. *Mol. Cell*, **62**, 745–755.
4. Pavlov,Y.I., Zhuk,A.S. and Stepchenkova,E.I. (2020) DNA polymerases at the eukaryotic replication fork thirty years after: connection to cancer. *Cancers (Basel)*, **12**. 3489.
5. Reha-Krantz,L.J. (2010) DNA polymerase proofreading: multiple roles maintain genome stability. *Biochim. Biophys. Acta*, **1804**, 1049–1063.
6. Mathews,C.K. (2006) DNA precursor metabolism and genomic stability. *FASEB J.*, **20**, 1300–1314.
7. Niida,H., Shimada,M., Murakami,H. and Nakanishi,M. (2010) Mechanisms of dNTP supply that play an essential role in maintaining genome integrity in eukaryotic cells. *Cancer Sci.*, **101**, 2505–2509.
8. Mathews,C.K. (2015) Deoxyribonucleotide metabolism, mutagenesis and cancer. *Nat. Rev. Cancer*, **15**, 528–539.
9. Pai,C.C. and Kearsey,S. (2017) A critical balance: dNTPs and the maintenance of genome stability. *Genes*, **8**, 57.
10. Chabes,A., Georgieva,B., Domkin,V., Zhao,X., Rothstein,R. and Thelander,L. (2003) Survival of DNA damage in yeast directly depends on increased dNTP levels allowed by relaxed feedback inhibition of ribonucleotide reductase. *Cell*, **112**, 391–401.
11. Wheeler,L.J., Rajagopal,I. and Mathews,C.K. (2005) Stimulation of mutagenesis by proportional deoxyribonucleoside triphosphate accumulation in *Escherichia coli*. *DNA Repair (Amst.)*, **4**, 1450–1456.
12. Gon,S., Napolitano,R., Rocha,W., Coulon,S. and Fuchs,R.P. (2011) Increase in dNTP pool size during the DNA damage response plays a key role in spontaneous and induced-mutagenesis in *Escherichia coli*. *Proc. Natl. Acad. Sci. U.S.A.*, **108**, 19311–19316.
13. Kochenova,O.V., Bezalel-Buch,R., Tran,P., Makarova,A.V., Chabes,A., Burgers,P.M. and Shcherbakova,P.V. (2017) Yeast DNA polymerase ζ maintains consistent activity and mutagenicity across a wide range of physiological dNTP concentrations. *Nucleic Acids Res.*, **45**, 1200–1218.
14. Northam,M.R., Robinson,H.A., Kochenova,O.V. and Shcherbakova,P.V. (2010) Participation of DNA polymerase ζ in replication of undamaged DNA in *Saccharomyces cerevisiae*. *Genetics*, **184**, 27–42.
15. The Cancer Genome Atlas Network (2012) Comprehensive molecular characterization of human colon and rectal cancer. *Nature*, **487**, 330–337.
16. The Cancer Genome Atlas Research Network (2013) Integrated genomic characterization of endometrial carcinoma. *Nature*, **497**, 67–73.
17. Rayner,E., van Gool,I.C., Palles,C., Kearsey,S.E., Bosse,T., Tomlinson,I. and Church,D.N. (2016) A panoply of errors: polymerase proofreading domain mutations in cancer. *Nat. Rev. Cancer*, **16**, 71–81.
18. Barbari,S.R. and Shcherbakova,P.V. (2017) Replicative DNA polymerase defects in human cancers: consequences, mechanisms, and implications for therapy. *DNA Repair (Amst.)*, **56**, 16–25.
19. Kane,D.P. and Shcherbakova,P.V. (2014) A common cancer-associated DNA polymerase ε mutation causes an exceptionally strong mutator phenotype, indicating fidelity defects distinct from loss of proofreading. *Cancer Res.*, **74**, 1895–1901.
20. Barbari,S.R., Kane,D.P., Moore,E.A. and Shcherbakova,P.V. (2018) Functional analysis of cancer-associated DNA polymerase ε variants in *Saccharomyces cerevisiae*. *G3 (Bethesda)*, **8**, 1019–1029.
21. Li,H.D., Cuevas,I., Zhang,M., Lu,C., Alam,M.M., Fu,Y.X., You,M.J., Akbay,E.A., Zhang,H. and Castrillon,D.H. (2018) Polymerase-mediated ultramutagenesis in mice produces diverse cancers with high mutational load. *J. Clin. Invest.*, **128**, 4179–4191.
22. Xing,X., Kane,D.P., Bulock,C.R., Moore,E.A., Sharma,S., Chabes,A. and Shcherbakova,P.V. (2019) A recurrent cancer-associated substitution in DNA polymerase ε produces a hyperactive enzyme. *Nat. Commun.*, **10**, 374.
23. Galati,M.A., Hodel,K.P., Gams,M.S., Sudhaman,S., Bridge,T., Zahurancik,W.J., Ungerleider,N.A., Park,V.S., Ercan,A.B.,

Joksimovic,L. *et al.* (2020) Cancers from novel *Pole*-mutant mouse models provide insights into polymerase-mediated hypermutagenesis and immune checkpoint blockade. *Cancer Res.*, **80**, 5606–5618.
24. Herzog,M., Alonso-Perez,E., Salguero,I., Warringer,J., Adams,D.J., Jackson,S.P. and Puddu,F. (2021) Mutagenic mechanisms of cancer-associated DNA polymerase ε alleles. *Nucleic Acids Res.*, **49**, 3919–3931.
25. Li,H.D., Lu,C., Zhang,H., Hu,Q., Zhang,J., Cuevas,I.C., Sahoo,S.S., Aguilar,M., Maurais,E.G., Zhang,S. *et al.* (2020) A *Pole*^{P286R} mouse model of endometrial cancer recapitulates high mutational burden and immunotherapy response. *JCI Insight*, **5**, e138829.
26. Albertson,T.M., Ogawa,M., Bugni,J.M., Hays,L.E., Chen,Y., Wang,Y., Treuting,P.M., Heddle,J.A., Goldsby,R.E. and Preston,B.D. (2009) DNA polymerase ε and δ proofreading suppress discrete mutator and cancer phenotypes in mice. *Proc. Natl. Acad. Sci. U.S.A.*, **106**, 17101–17104.
27. Shinbrot,E., Henninger,E.E., Weinhold,N., Covington,K.R., Göksenin,A.Y., Schultz,N., Chao,H., Doddapaneni,H., Muzny,D.M., Gibbs,R.A. *et al.* (2014) Exonuclease mutations in DNA polymerase ε reveal replication strand specific mutation patterns and human origins of replication. *Genome Res.*, **24**, 1740–1750.
28. Parkash,V., Kulkarni,Y., Ter Beek,J., Shcherbakova,P.V., Kamerlin,S.C.L. and Johansson,E. (2019) Structural consequence of the most frequently recurring cancer-associated substitution in DNA polymerase ε. *Nat. Commun.*, **10**, 373.
29. Gary,J.D. and Clarke,S. (1995) Purification and characterization of an isoaspartyl dipeptidase from *Escherichia coli*. *J. Biol. Chem.*, **270**, 4076–4087.
30. Morrison,A., Bell,J.B., Kunkel,T.A. and Sugino,A. (1991) Eukaryotic DNA polymerase amino acid sequence required for 3′→5′ exonuclease activity. *Proc. Natl. Acad. Sci. U.S.A.*, **88**, 9473–9477.
31. Chilkova,O., Jonsson,B.H. and Johansson,E. (2003) The quaternary structure of DNA polymerase ε from *Saccharomyces cerevisiae*. *J. Biol. Chem.*, **278**, 14082–14086.
32. Shcherbakova,P.V. and Kunkel,T.A. (1999) Mutator phenotypes conferred by *MLH1* overexpression and by heterozygosity for *mlh1* mutations. *Mol. Cell. Biol.*, **19**, 3177–3183.
33. Mertz,T.M., Sharma,S., Chabes,A. and Shcherbakova,P.V. (2015) Colon cancer-associated mutator DNA polymerase δ variant causes expansion of dNTP pools increasing its own infidelity. *Proc. Natl. Acad. Sci. U.S.A.*, **112**, E2467–E2476.
34. Jain,R., Vanamee,E.S., Dzikovski,B.G., Buku,A., Johnson,R.E., Prakash,L., Prakash,S. and Aggarwal,A.K. (2014) An iron-sulfur cluster in the polymerase domain of yeast DNA polymerase ε. *J. Mol. Biol.*, **426**, 301–308.
35. McCoy,A.J., Grosse-Kunstleve,R.W., Adams,P.D., Winn,M.D., Storoni,L.C. and Read,R.J. (2007) Phaser crystallographic software. *J. Appl. Crystallogr.*, **40**, 658–674.
36. Hogg,M., Osterman,P., Bylund,G.O., Ganai,R.A., Lundström,E.B., Sauer-Eriksson,A.E. and Johansson,E. (2014) Structural basis for processive DNA synthesis by yeast DNA polymerase ε. *Nat. Struct. Mol. Biol.*, **21**, 49–55.
37. Emsley,P., Lohkamp,B., Scott,W.G. and Cowtan,K. (2010) Features and development of coot. *Acta. Crystallogr. D Biol. Crystallogr.*, **66**, 486–501.
38. Adams,P.D., Afonine,P.V., Bunkoczi,G., Chen,V.B., Davis,I.W., Echols,N., Headd,J.J., Hung,L.W., Kapral,G.J., Grosse-Kunstleve,R.W. *et al.* (2010) PHENIX: a comprehensive Python-based system for macromolecular structure solution. *Acta. Crystallogr. D Biol. Crystallogr.*, **66**, 213–221.
39. Chen,V.B., Arendall,W.B. 3rd, Headd,J.J., Keedy,D.A., Immormino,R.M., Kapral,G.J., Murray,L.W., Richardson,J.S. and Richardson,D.C. (2010) MolProbity: all-atom structure validation for macromolecular crystallography. *Acta. Crystallogr. D Biol. Crystallogr.*, **66**, 12–21.
40. Palles,C., Cazier,J.B., Howarth,K.M., Domingo,E., Jones,A.M., Broderick,P., Kemp,Z., Spain,S.L., Guarino,E., Salguero,I. *et al.* (2013) Germline mutations affecting the proofreading domains of POLE and POLD1 predispose to colorectal adenomas and carcinomas. *Nat. Genet.*, **45**, 136–144.
41. Valle,L., Hernández-Illán,E., Bellido,F., Aiza,G., Castillejo,A., Castillejo,M.I., Navarro,M., Seguí,N., Vargas,G., Guarinos,C. *et al.* (2014) New insights into *POLE* and *POLD1* germline mutations in familial colorectal cancer and polyposis. *Hum. Mol. Genet.*, **23**, 3506–3512.
42. Grossman,R.L., Heath,A.P., Ferretti,V., Varmus,H.E., Lowy,D.R., Kibbe,W.A. and Staudt,L.M. (2016) Toward a shared vision for cancer genomic data. *N. Engl. J. Med.*, **375**, 1109–1112.
43. Church,D.N., Briggs,S.E., Palles,C., Domingo,E., Kearsey,S.J., Grimes,J.M., Gorman,M., Martin,L., Howarth,K.M., Hodgson,S.V. *et al.* (2013) DNA polymerase ε and δ exonuclease domain mutations in endometrial cancer. *Hum. Mol. Genet.*, **22**, 2820–2828.
44. Campbell,B.B., Light,N., Fabrizio,D., Zatzman,M., Fuligni,F., de Borja,R., Davidson,S., Edwards,M., Elvin,J.A., Hodel,K.P. *et al.* (2017) Comprehensive analysis of hypermutation in human cancer. *Cell*, **171**, 1042–1056.
45. Alexandrov,L.B., Nik-Zainal,S., Wedge,D.C., Aparicio,S.A., Behjati,S., Biankin,A.V., Bignell,G.R., Bolli,N., Borg,A., Borresen-Dale,A.L. *et al.* (2013) Signatures of mutational processes in human cancer. *Nature*, **500**, 415–421.
46. Hussein,Y.R., Weigelt,B., Levine,D.A., Schoolmeester,J.K., Dao,L.N., Balzer,B.L., Liles,G., Karlan,B., Kobel,M., Lee,C.H. *et al.* (2015) Clinicopathological analysis of endometrial carcinomas harboring somatic *POLE* exonuclease domain mutations. *Mod. Pathol.*, **28**, 505–514.
47. Bellone,S., Centritto,F., Black,J., Schwab,C., English,D., Cocco,E., Lopez,S., Bonazzoli,E., Predolini,F., Ferrari,F. *et al.* (2015) Polymerase ε (POLE) ultra-mutated tumors induce robust tumor-specific CD4+ t cell responses in endometrial cancer patients. *Gynecol. Oncol.*, **138**, 11–17.
48. McAlpine,J.N., Chiu,D.S., Nout,R.A., Church,D.N., Schmidt,P., Lam,S., Leung,S., Bellone,S., Wong,A., Brucker,S.Y. *et al.* (2021) Evaluation of treatment effects in patients with endometrial cancer and *POLE* mutations: an individual patient data meta-analysis. *Cancer*, **127**, 2409–2422.
49. Jumaah,A.S., Salim,M.M., Al-Haddad,H.S., McAllister,K.A. and Yasseen,A.A. (2020) The frequency of POLE-mutation in endometrial carcinoma and prognostic implications: a systemic review and meta-analysis. *J. Pathol. Transl. Med.*, **54**, 471–479.
50. Howitt,B.E., Shukla,S.A., Sholl,L.M., Ritterhouse,L.L., Watkins,J.C., Rodig,S., Stover,E., Strickland,K.C., D'Andrea,A.D., Wu,C.J. *et al.* (2015) Association of polymerase ε-mutated and microsatellite-instable endometrial cancers with neoantigen load, number of tumor-infiltrating lymphocytes, and expression of PD-1 and PD-L1. *JAMA Oncol.*, **1**, 1319–1323.
51. Gong,J., Wang,C., Lee,P.P., Chu,P. and Fakih,M. (2017) Response to PD-1 blockade in microsatellite stable metastatic colorectal cancer harboring a *POLE* mutation. *J. Natl. Compr. Canc. Netw.*, **15**, 142–147.
52. Mehnert,J.M., Panda,A., Zhong,H., Hirshfield,K., Damare,S., Lane,K., Sokol,L., Stein,M.N., Rodriguez-Rodriquez,L., Kaufman,H.L. *et al.* (2016) Immune activation and response to pembrolizumab in *POLE*-mutant endometrial cancer. *J. Clin. Invest.*, **126**, 2334–2340.
53. Wimmer,K., Beilken,A., Nustede,R., Ripperger,T., Lamottke,B., Ure,B., Steinmann,D., Reineke-Plaass,T., Lehmann,U., Zschocke,J. *et al.* (2017) A novel germline *POLE* mutation causes an early onset cancer prone syndrome mimicking constitutional mismatch repair deficiency. *Fam. Cancer*, **16**, 67–71.
54. Shcherbakova,P.V., Pavlov,Y.I., Chilkova,O., Rogozin,I.B., Johansson,E. and Kunkel,T.A. (2003) Unique error signature of the four-subunit yeast DNA polymerase ε. *J. Biol. Chem.*, **278**, 43770–43780.
55. Williams,L.N., Marjavaara,L., Knowels,G.M., Schultz,E.M., Fox,E.J., Chabes,A. and Herr,A.J. (2015) dNTP pool levels modulate mutator phenotypes of error-prone DNA polymerase ε variants. *Proc. Natl. Acad. Sci. U.S.A.*, **112**, E2457–E2466.
56. Mirkin,E.V. and Mirkin,S.M. (2007) Replication fork stalling at natural impediments. *Microbiol. Mol. Biol. Rev.*, **71**, 13–35.
57. Treangen,T.J. and Salzberg,S.L. (2011) Repetitive DNA and next-generation sequencing: computational challenges and solutions. *Nat. Rev. Genet.*, **13**, 36–46.
58. Northam,M.R., Moore,E.A., Mertz,T.M., Binz,S.K., Stith,C.M., Stepchenkova,E.I., Wendt,K.L., Burgers,P.M. and Shcherbakova,P.V. (2014) DNA polymerases ζ and Rev1 mediate error-prone bypass of non-B DNA structures. *Nucleic Acids Res.*, **42**, 290–306.

59. Ganai,R.A., Zhang,X.P., Heyer,W.D. and Johansson,E. (2016) Strand displacement synthesis by yeast DNA polymerase ε. *Nucleic Acids Res.*, **44**, 8229–8240.
60. Tran,H.T., Keen,J.D., Kricker,M., Resnick,M.A. and Gordenin,D.A. (1997) Hypermutability of homonucleotide runs in mismatch repair and DNA polymerase proofreading yeast mutants. *Mol. Cell. Biol.*, **17**, 2859–2865.
61. Williams,L.N., Herr,A.J. and Preston,B.D. (2013) Emergence of DNA polymerase ε antimutators that escape error-induced extinction in yeast. *Genetics*, **193**, 751–770.
62. Bulock,C.R., Xing,X. and Shcherbakova,P.V. (2020) Mismatch repair and DNA polymerase δ proofreading prevent catastrophic accumulation of leading strand errors in cells expressing a cancer-associated DNA polymerase ε variant. *Nucleic Acids Res.*, **48**, 9124–9134.
63. Morrison,A. and Sugino,A. (1994) The 3′→5′ exonucleases of both DNA polymerases δ and ε participate in correcting errors of DNA replication in *Saccharomyces cerevisiae*. *Mol. Gen. Genet.*, **242**, 289–296.
64. Kirchner,J.M., Tran,H. and Resnick,M.A. (2000) A DNA polymerase ε mutant that specifically causes +1 frameshift mutations within homonucleotide runs in yeast. *Genetics*, **155**, 1623–1632.
65. Pavlov,Y.I., Shcherbakova,P.V. and Kunkel,T.A. (2001) *In vivo* consequences of putative active site mutations in yeast DNA polymerases α, ε, δ, and ζ. *Genetics*, **159**, 47–64.
66. Davidson,R.L., Broeker,P. and Ashman,C.R. (1988) DNA base sequence changes and sequence specificity of bromodeoxyuridine-induced mutations in mammalian cells. *Proc. Natl. Acad. Sci. U.S.A.*, **85**, 4406–4410.
67. Reha-Krantz,L.J. and Liesner,E.M. (1984) Mutagenic specificity of a novel T4 DNA polymerase mutant. *Genetics*, **106**, 335–345.
68. Shcherbakova,P.V. and Pavlov,Y.I. (1993) Mutagenic specificity of the base analog 6-*N*-hydroxylaminopurine in the *URA3* gene of the yeast *Saccharomyces cerevisiae*. *Mutagenesis*, **8**, 417–421.
69. Daee,D.L., Mertz,T.M. and Shcherbakova,P.V. (2010) A cancer-associated DNA polymerase δ variant modeled in yeast causes a catastrophic increase in genomic instability. *Proc. Natl. Acad. Sci. U.S.A.*, **107**, 157–162.
70. Briggs,S. and Tomlinson,I. (2013) Germline and somatic polymerase ε and δ mutations define a new class of hypermutated colorectal and endometrial cancers. *J. Pathol.*, **230**, 148–153.
71. Stocki,S.A., Nonay,R.L. and Reha-Krantz,L.J. (1995) Dynamics of bacteriophage T4 DNA polymerase function: identification of amino acid residues that affect switching between polymerase and 3′→5′ exonuclease activities. *J. Mol. Biol.*, **254**, 15–28.
72. Snyder,A. and Wolchok,J.D. (2016) Successful treatment of a patient with glioblastoma and a germline *POLE* mutation: where next?*Cancer Discov.*, **6**, 1210–1211.
73. Johanns,T.M., Miller,C.A., Dorward,I.G., Tsien,C., Chang,E., Perry,A., Uppaluri,R., Ferguson,C., Schmidt,R.E., Dahiya,S. *et al.* (2016) Immunogenomics of hypermutated glioblastoma: a patient with germline *POLE* deficiency treated with checkpoint blockade immunotherapy. *Cancer Discov.*, **6**, 1230–1236.
74. Santin,A.D., Bellone,S., Centritto,F., Schlessinger,J. and Lifton,R. (2015) Improved survival of patients with hypermutation in uterine serous carcinoma. *Gynecol. Oncol. Rep.*, **12**, 3–4.
75. Santin,A.D., Bellone,S., Buza,N., Choi,J., Schwartz,P.E., Schlessinger,J. and Lifton,R.P. (2016) Regression of chemotherapy-resistant polymerase ε (POLE) ultra-mutated and MSH6 hyper-mutated endometrial tumors with nivolumab. *Clin. Cancer Res.*, **22**, 5682–5687.
76. Muzyczka,N., Poland,R.L. and Bessman,M.J. (1972) Studies on the biochemical basis of spontaneous mutation. I. A comparison of the deoxyribonucleic acid polymerases of mutator, antimutator, and wild type strains of bacteriophage t4. *J. Biol. Chem.*, **247**, 7116–7122.
77. Gillin,F.D. and Nossal,N.G. (1976) Control of mutation frequency by bacteriophage T4 DNA polymerase. II. Accuracy of nucleotide selection by the L88 mutator, CB120 antimutator, and wild type phage T4 DNA polymerases. *J. Biol. Chem.*, **251**, 5225–5232.
78. Reha-Krantz,L.J. (1995) Learning about DNA polymerase function by studying antimutator DNA polymerases. *Trends Biochem. Sci*, **20**, 136–140.
79. Reha-Krantz,L.J. and Nonay,R.L. (1993) Genetic and biochemical studies of bacteriophage T4 DNA polymerase 3′→5′-exonuclease activity. *J. Biol. Chem.*, **268**, 27100–27108.
80. Reha-Krantz,L.J. (1998) Regulation of DNA polymerase exonucleolytic proofreading activity: studies of bacteriophage T4 'antimutator' DNA polymerases. *Genetics*, **148**, 1551–1557.
81. Reha-Krantz,L.J. and Nonay,R.L. (1994) Motif a of bacteriophage T4 DNA polymerase: role in primer extension and DNA replication fidelity. Isolation of new antimutator and mutator DNA polymerases. *J. Biol. Chem.*, **269**, 5635–5643.
82. Temko,D., Van Gool,I.C., Rayner,E., Glaire,M., Makino,S., Brown,M., Chegwidden,L., Palles,C., Depreeuw,J., Beggs,A. *et al.* (2018) Somatic *POLE* exonuclease domain mutations are early events in sporadic endometrial and colorectal carcinogenesis, determining driver mutational landscape, clonal neoantigen burden and immune response. *J. Pathol.*, **245**, 283–296.
83. Bester,A.C., Roniger,M., Oren,Y.S., Im,M.M., Sarni,D., Chaoat,M., Bensimon,A., Zamir,G., Shewach,D.S. and Kerem,B. (2011) Nucleotide deficiency promotes genomic instability in early stages of cancer development. *Cell*, **145**, 435–446.
84. Aird,K.M., Zhang,G., Li,H., Tu,Z., Bitler,B.G., Garipov,A., Wu,H., Wei,Z., Wagner,S.N., Herlyn,M. *et al.* (2013) Suppression of nucleotide metabolism underlies the establishment and maintenance of oncogene-induced senescence. *Cell Rep.*, **3**, 1252–1265.
85. Datta,A., Schmeits,J.L., Amin,N.S., Lau,P.J., Myung,K. and Kolodner,R.D. (2000) Checkpoint-dependent activation of mutagenic repair in *Saccharomyces cerevisiae pol3-01* mutants. *Mol. Cell*, **6**, 593–603.
86. Gouge,J., Ralec,C., Henneke,G. and Delarue,M. (2012) Molecular recognition of canonical and deaminated bases by *P. abyssi* family B DNA polymerase. *J. Mol. Biol.*, **423**, 315–336.